

ORIGINAL ARTICLE

Sphaerosiderites as sensitive recorders of non-marine depositional and diagenetic history: Insights from the Lower Cretaceous Wealden Supergroup

Ritwika Sengupta¹  | Stuart A. Robinson¹  | Nicholas J. Tosca² ¹Department of Earth Sciences,
University of Oxford, Oxford, UK²Department of Earth Sciences,
University of Cambridge, Cambridge, UK**Correspondence**Stuart A. Robinson, Department of Earth
Sciences, University of Oxford, Oxford
OX1 3AN, UK.

Email: stuart.robinson@earth.ox.ac.uk

Funding informationNatural Environment Research Council,
Grant/Award Number: NE/L002612/1**Abstract**

Waterlogged, reducing soils in modern and ancient wetlands feature distinctive syndepositional to early diagenetic spherical iron carbonate concretions, known as sphaerosiderites. Sphaerosiderites are thought to record pore water elemental chemistry and local palaeoenvironmental conditions, and are widely used in palaeohydrological reconstructions throughout the Phanerozoic. The Lower Cretaceous non-marine Wealden Supergroup of Southern England, deposited in fluvio-lacustrine settings, contains abundant well-preserved sphaerosiderites offering an ideal archive for unravelling the geochemistry of ancient non-marine environments. Sphaerosiderites were characterised via multiple microanalytical techniques (SEM-EDS, EPMA, XRD, SIMS), and show morphological and compositional heterogeneity (e.g. concentric zones of variably enriched Mn, Ca or Mg, elemental differences between cores and rims) in well-preserved sphaerosiderites from the Ashdown and Tunbridge Wells Sand formations. The preservation of primary fabrics, lack of post-burial cements or extensive alteration suggests these sphaerosiderites record primary palaeoenvironmental conditions. By contrast, in the Wadhurst Clay Formation, sphaerosiderites are recrystallised, potentially reflecting wide scale palaeoenvironmental changes (e.g. marine incursions). New experimental constraints on elemental uptake during siderite growth suggests that rather than reflecting pore water elemental chemistry, the elemental heterogeneity in the Wealden sphaerosiderites reflects complex parameters; variations in pH, cation concentrations, DIC, growth rate and siderite saturation state in groundwaters. At a larger scale, morphological and compositional differences between sphaerosiderites from distinct palaeosol horizons record spatial and temporal variability in local hydrogeochemistry. This suggests that the Weald Basin wetlands of the Lower Cretaceous featured a dynamic and periodically fluctuating groundwater table, where sphaerosiderites growing close to the soil surface responded rapidly to variability in physiochemical conditions, consistent with wet and warm conditions suggested by sedimentological evidence and climate model simulations. Similar morphological and compositional

This is an open access article under the terms of the Creative Commons Attribution License, which permits use, distribution and reproduction in any medium, provided the original work is properly cited.

© 2021 The Authors. *The Depositional Record* published by John Wiley & Sons Ltd on behalf of International Association of Sedimentologists

variability noted in other Phanerozoic sphaerosiderites suggests analogous processes operated in ancient wetlands, and that sphaerosiderites could provide a crucial tool to understand wetland dynamics in deep time.

KEYWORDS

Cretaceous, siderite, sphaerosiderites, Wealden

1 | INTRODUCTION

Sphaerosiderites, spherical iron carbonate precipitates that can reach several hundred microns in size, are well known diagenetic products of waterlogged, reducing soils in modern and ancient wetland environments (Choi et al., 2003; Driese et al., 2010; Khim et al., 1999, 2000; Ludvigson et al., 1998, 2013; Moore et al., 1992; Mozley & Wersin, 1992; Pye et al., 1990; Ufnar et al., 2004a,b). Owing in part to their robust mineralogy and depositional setting, sphaerosiderites are thought to record key parameters of pore water chemistry and the oxygen isotopic composition ($\delta^{18}\text{O}$) of meteoric groundwaters, and as a consequence are widely used for palaeoenvironmental and palaeohydrological reconstructions (Choi et al., 2003; Khim et al., 1999; Ludvigson et al., 1998; Passey, 2014; Robinson et al., 2010; Suarez et al., 2010; Ufnar et al., 2004a,b; Weibel et al., 2016).

Early geochemical studies hypothesised that the elemental composition of siderite should reflect the chemistry of the growth solution (i.e. palaeo pore waters) (Mozley, 1989). On this basis, extensive substitution of Mg or Ca in siderite has been interpreted as reflecting the influence of marine conditions while low Mg or Ca and higher Mn has been thought to indicate growth in freshwaters (Mozley, 1989). As a consequence, this first-order classification/interpretation scheme has been widely applied to Phanerozoic siderites in order to evaluate their suitability as palaeoenvironmental proxies (Choi et al., 2003; Choi & Kim, 2006; Ludvigson et al., 2013; Mozley, 1989; Robinson et al., 2010; Suarez et al., 2010; Ufnar et al., 2004b; Weibel et al., 2016). However, the majority of laboratory investigations (conducted at crystallisation rates orders of magnitude higher than natural settings) have failed to reproduce this clear compositional link between siderite and pore water chemistry (Carothers et al., 1988; Jimenez-Lopez & Romanek, 2004; Mortimer et al., 1997; Postma, 1980; Pye et al., 1990; Romanek et al., 2009; Steinmann & Shotyk, 1997; Thornber & Nickel, 1976). A recent experimental study more closely approximating sedimentary pore water geochemistry showed that siderite composition reflects a complex suite of palaeoenvironmental conditions including siderite saturation state, growth rate, cation

concentrations, pH and temperature (Sengupta et al., 2020). These new geochemical constraints are leveraged here through detailed characterisation of well-preserved sphaerosiderites from the Lower Cretaceous non-marine Wealden Supergroup, UK (Allen, 1975, 1981, 1989; Allen et al., 1998; Radley, 1994, 2006a, 2006b; Radley & Allen, 2012). Interpretation of sphaerosiderite petrography and geochemistry in an aqueous geochemical framework provides a more holistic overview of the growth conditions of these ancient siderites, and by extension, provides new perspectives on Lower Cretaceous non-marine palaeoenvironmental conditions during deposition of the Wealden Supergroup.

2 | MATERIALS AND METHODS

2.1 | The Wealden supergroup: lithostratigraphy and sampling

The non-marine Wealden Supergroup of Southern England was deposited during the Lower Cretaceous (Berriasian to Aptian) at 30–34°N palaeolatitude within the Weald-Wessex basins (Allen & Wimbledon, 1991; Horne, 1995; Morter, 1984; Worssam & Morter, 1978). The Wealden Supergroup comprises mainly sandstones and mudstones predominantly deposited in freshwater fluvial, floodplain and lagoonal environments, and provides an important Lower Cretaceous record of terrestrial palaeoenvironments, floras and faunas (Allen, 1975, 1981, 1989; Allen et al., 1998; Radley, 1994, 2006a, 2006b; Radley & Allen, 2012). Within the Weald Basin there are multiple well-preserved sphaerosiderite horizons within alternating argillaceous (Wadhurst Clay and Weald Clay formations) and arenaceous lithofacies (Ashdown and Tunbridge Wells Sand formations).

Sampling was undertaken from cores recovered from four boreholes within the Weald Basin (Fairlight, Cooden, Westfield and Cuckfield boreholes). The chosen cores were sampled at the British Geological Survey (BGS) Core Repository in Keyworth, UK and graphic logs of each borehole are presented in Figure 1, reconstructed using the original core sheets as continuous cores are no longer

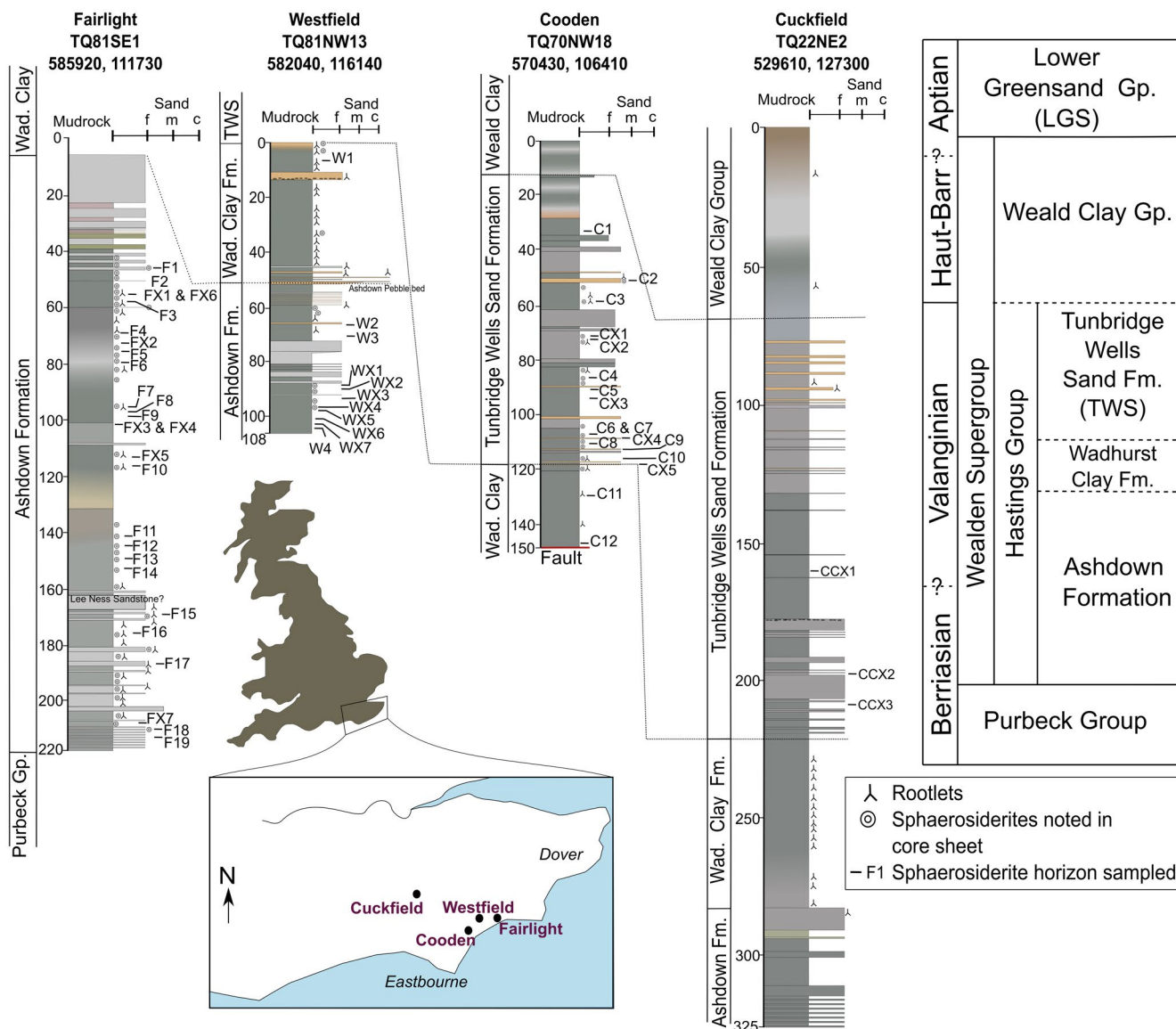


FIGURE 1 Lithostratigraphy and location of the sampled boreholes. Sphaerosiderite-bearing horizons were sampled from Cooden, Westfield, Fairlight and Cuckfield cores, and are marked at depth (metres). The graphic logs are reconstructed from log reports, and the colours denote colour changes noted within lithologies in the log reports (Geology of Britain, 2016; Lake, 1969; Shephard-Thorn et al., 1971; Thorley, 1969)

available (log reports available from the BGS ‘Geology of Britain’ online database (Geology of Britain, 2016; Lake, 1969; Shephard-Thorn et al., 1971; Thorley, 1969). In some palaeosol horizons, due to restrictions on sampling, only small (1 cm length pieces) could be taken. Based on preservation and a desire to maximise the stratigraphic resolution within each lithostratigraphic unit, 50 sphaerosiderite horizons were chosen (across all boreholes). Representative sphaerosiderite samples were collected from the Cooden, Westfield, Fairlight and Cuckfield boreholes spanning the Ashdown, Wadhurst Clay and Tunbridge Wells Sand formations. The stratigraphic position of each collected sample was recorded according to depth within the borehole it

was collected from, and the stratigraphic unit within the Wealden Supergroup (Data S1).

2.2 | Sample preparation and analytical techniques

Individual sphaerosiderites were picked by placing the bulk samples in de-ionized (DI) water for 10 min, allowing the matrix to soften. Spheres could then be picked individually from each sphaerosiderite horizon and air dried at room temperature for 5 min on a Petri dish. For analysis with scanning electron microscope (SEM) and electron

microprobe analyser (EPMA), sphaerosiderites were set in a 10 mm resin round and hand polished using diamond pads; the final polish was achieved using a 1 μm grade diamond pad. The rounds were cleaned between pads by submerging in isopropanol within a beaker placed in an ultrasonic bath for 5 min.

The rounds were imaged using a FEI Quanta 650 SEM in the Department of Earth Sciences at the University of Oxford to produce backscatter electron (BSE) and secondary electron (SE) images. The SEM is also equipped with an Oxford Instruments Energy-dispersive X-ray Spectroscopy (EDS) system used for element mapping at 20 kV. Although EDS does not allow a reliable quantification of all elements, it can produce maps of relative change in element concentrations. In the majority of horizons, up to five spheres were assessed via SEM in the time available. A CAMECA SX-5 FE EPMA was used for spot analyses along transects of spheres with spot sizes of 5 μm , and an acquisition time of 30 s at 15 kV, at 10 nA operating current. The elements of interest were Fe, Mn, Ca, Mg, Sr, Si, Na, Al, K, S and Ti. Data points which contained Al and Si oxide content >5 mol.% were removed as these data points within the transects were probably measuring incorporated inclusions within the sphaerosiderites. Data points with measurements below the detection limits of respective elements were also removed.

For powder X-ray diffraction (XRD), dried sphaerosiderites and bulk samples were crushed in an agate pestle and mortar to a fine powder. Powder was deposited as a slurry mixed with ethanol on a polished zero-background single crystal silicon substrate and air dried; this ensured relatively random particle orientation. The powders were analysed at University of Oxford using a PANalytical Empyrean Series 2 powder diffractometer using a Co K α source at 40 kV and 40 mA, scanned between 5 and 80° 2-theta at a step size of 0.026°. Raw powder diffraction data were analysed using Malvern Panalytical HighScore v4.9 and the International Center for Diffraction Data PDF-4+ database. This database includes updated and internally consistent reference intensity ratios for all minerals under consideration here and so mineral abundances are regarded as quantitative. External standards indicate that this analysis yields accurate results with uncertainties of ± 5 relative percent.

Thin sections were prepared for microscopy from 10 sphaerosiderite horizons, however, the poorly consolidated matrix prohibited adequate preparation of several samples for further microanalysis. However, a subset of suitable thin sections were used to identify phases, examine textures where possible, and provide petrographic context for the XRD mineralogical identification.

Three samples (FC5, FC9 and FC11) from the Ashdown Formation exposed in the coastal outcrop at

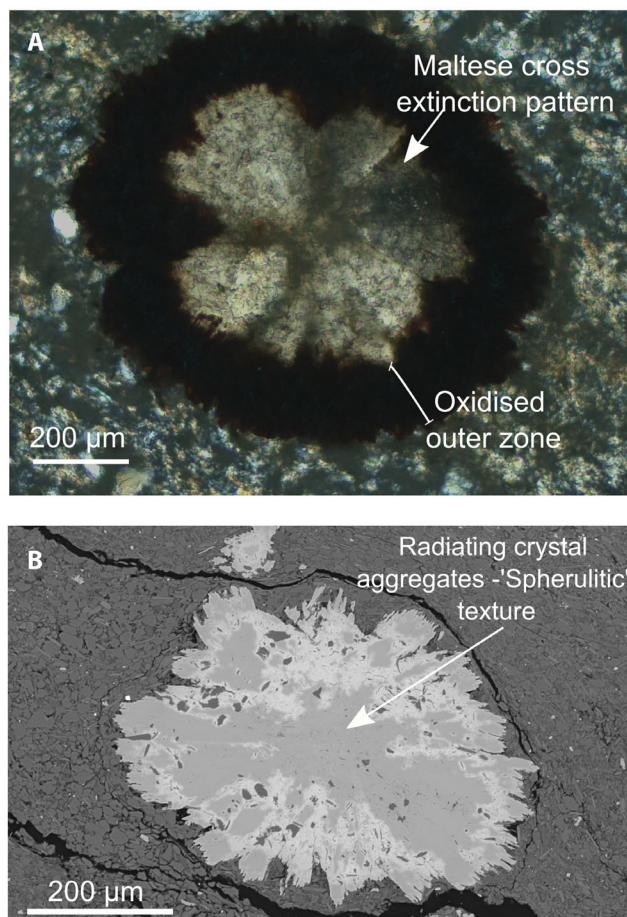


FIGURE 2 (A) Thin section photomicrographs in cross polarised light of sphaerosiderites from sample CX1 (Tunbridge Wells Sand) showing characteristic maltese cross extinction in the central part of the sphere and an oxidised rim. The matrix is composed mainly of quartz and clays. The thin section was thicker than 30 μm , and quartz appears yellow. (B) Backscatter (BSE) Imaging showing a different sphere of CX1 with compositional differences through contrast changes and spherulitic texture

Fairlight (previously reported in Robinson et al., 2010) were set in resin rounds and analysed using a Cameca IMS 1270 secondary ion mass spectrometry (SIMS) at the NERC (Natural Environment Research Council) facility at University of Edinburgh to produce $\delta^{18}\text{O}_{\text{siderite}}$ and $\delta^{13}\text{C}_{\text{siderite}}$ transects. The accelerating voltage was 10 kV, ca 10–15 μm Cs+ beam size, with an operating current of 5 nA, and an electron flood gun used for charge neutralisation. Oxygen isotope measurements were conducted in multi collection mode and used multi collector and Faraday Cups (L'1) and (H'1), and carbon isotope measurements (mono collection) used peak switching between detectors FC2 and EM.

Three samples from a batch of Ivigtut siderite provided by NERC at University of Edinburgh were set in the resin round with the Wealden samples. The Ivigtut siderite was

analysed alongside the samples and used to correct the sphaerosiderite values, based on the NERC facility's own measurements of Ivigtut. The precision for carbon was $\pm 0.3\%$ (1σ), and for oxygen $\pm 0.6\%$ (1σ), based on 15 point analyses on each of the three Ivigtut samples.

3 | RESULTS

3.1 | Thin section and SEM

3.1.1 | Sphaerosiderite mineralogy and morphology

In the limited available thin sections, the matrix consists mainly of clays and quartz. No petrographic evidence of carbonate cements was found in the matrix (Figure 2). The sphaerosiderites are yellow to brown in colour in cross polarized light and 100 μm to 1 mm in diameter. In thin section and SEM images, the sphaerosiderites exhibit a variety of morphologies which are classified into five types; 1a to 1e as described in Table 1 and displayed in Figure 3.

Morphological variations include a variety of internal zonations, including outward-radiating siderite crystal aggregates (often termed 'spherulitic' and exhibiting the characteristic Maltese cross extinction pattern) (Figures 2A and 3C), a distinct core and a rim (microcrystalline core and a spherulitic or bladed outer rim; Figure 3A), or multiple concentric growth and/or oxidation zones within individual spheres (Figure 3B). Some sphaerosiderites also appear homogenous, with no obvious internal zonation, as evidenced by the lack of contrast changes during BSE analysis across the sphere (Figure 3E). A limited number of horizons contain recrystallised sphaerosiderites (Figure 3F). The key observation is that morphological heterogeneity between horizons is common and varies

temporally and spatially (Figure 3), but spheres from the same hand sample (i.e. same palaeosol horizon) consistently show similar morphology.

The proportion of mineral inclusions varies within the sphaerosiderites (0–80 wt% inclusions, from XRD, Supplementary Information Section 2.1.1). These inclusions are randomly orientated, and were probably incorporated as siderite spheres grew around them. The number and type of inclusions incorporated within the spheres of any horizon are influenced by the matrix in which the sphere grew. The dominant inclusion mineralogy in these sphaerosiderites is quartz, but clays comprise up to 5%–15% of the inclusions (kaolinite, illite and small amounts of muscovite). Minor pyrite (<1%) is present in some of the sphaerosiderite horizons, visible as high contrast specks (<0.5 μm) within sphaerosiderites in BSE images and opaque grains in polarized light images. Two sphaerosiderite horizons contain larger pyrite inclusions that are up to 20 μm in diameter. These larger pyrite inclusions are spherical to sub spherical, with a microcrystalline centre and blocky outer rims, and contain inclusions within themselves of angular elongated siderite and minor quartz and clays (discussed further in Section 3.4.1). Pyrite is generally associated with sphaerosiderites and largely absent from the matrix, indicating that the pyrite formation is most probably linked to the formation of the sphaerosiderites.

3.1.2 | Recrystallisation textures in the Wadhurst Clay Formation

In the Wadhurst Clay Formation, the sphaerosiderite-bearing palaeosol horizons observed are limited in number, poorly preserved and oxidised. In the top 40 m of the Wadhurst Clay in both Cooden and Westfield boreholes, sphaerosiderites are either partially or wholly

TABLE 1 Descriptions of morphological types within Wealden sphaerosiderites

Morphology type	Figure	Description	Variations
1a	Figure 3A	Core-rim morphology change, usually with a microcrystalline core and a spherulitic or bladed outer rim	Rims can also have a blocky morphology
1b	Figure 3B	Multiple concentric zones of varying diameter within the spherule	Can be oxidation zones within the spherule
1c	Figure 3C,D	Spherulitic texture	Depending on the crystal face, can also appear as angular changes in contrast in BSE
1d	Figure 3E	Appears homogenous, no internal zonation	Can be internally homogenous, with small (<5 μm) spherulitic texture noted at rims, or a mottled contrast change within a cryptocrystalline sphere
1e	Figure 3F	Diagenetically altered	Wholly or partially recrystallised, and/or parts of the sphere have undergone dissolution

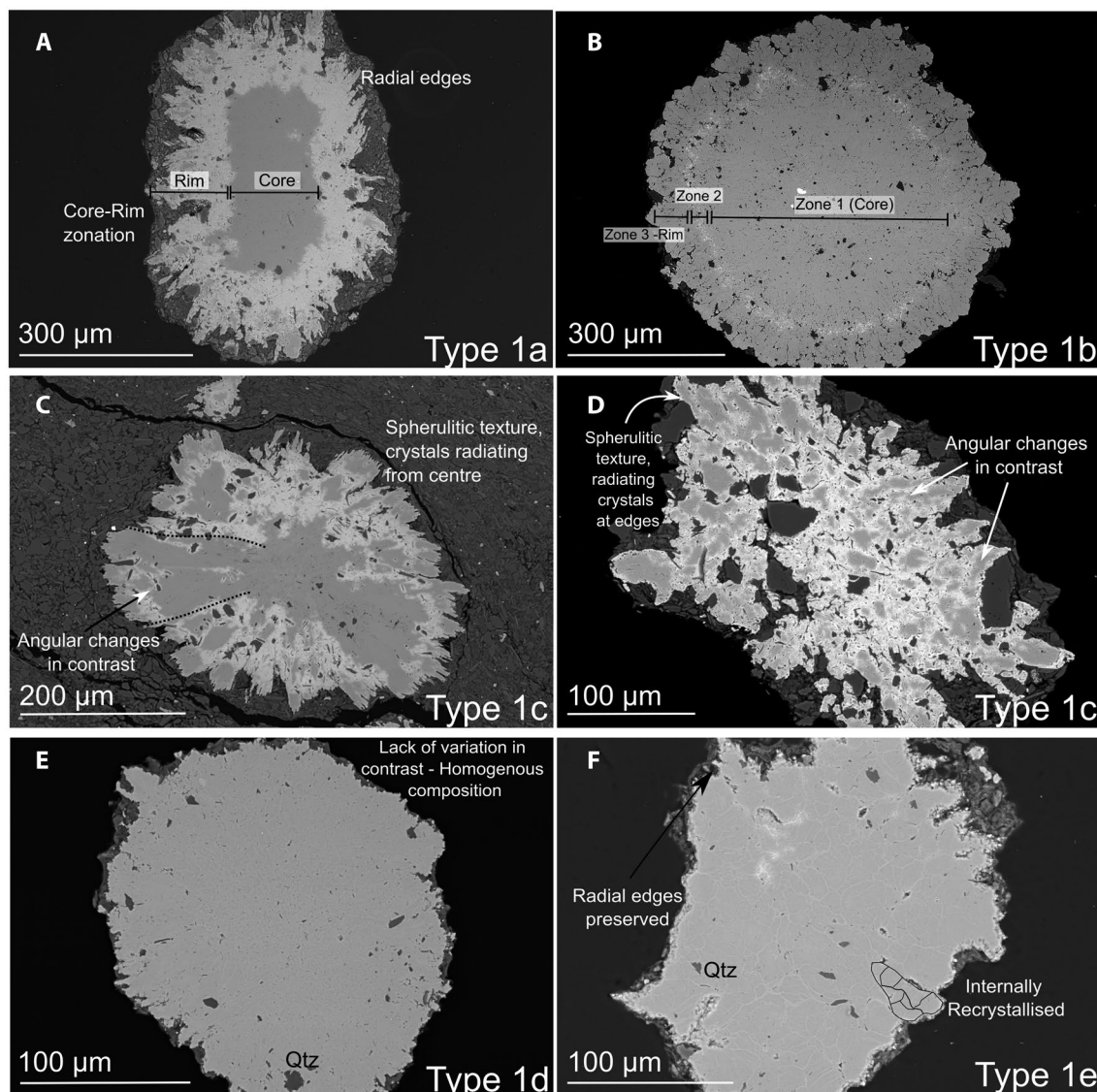


FIGURE 3 BSE images of representative sphaerosiderite morphology types from (A) Sample F11 (Ashdown Fm., Fairlight borehole) with distinct core and rim with radial edges, (B) Sample FC5 from Robinson et al. (2010) (Ashdown Fm.) containing multiple growth zones, (C) Sample W2 (Ashdown Fm., Westfield borehole) with spherulitic texture, (D) Sample F3 (Ashdown Fm., Fairlight borehole) containing angular blocks of compositional change and spherulitic edges, (E) Sphere from F18 (Ashdown Fm., Westfield borehole) which appears homogenous, (F) Sample C11 (Wadhurst Clay Fm., Cooden borehole) which is wholly recrystallised, but preserves the original spherulite shapes

recrystallised (Figure 4). Recrystallisation was identifiable by the presence of interlocking blocky siderite crystals visible in BSE images within spheres (20–100 μm edges), which were randomly orientated within the sphere, as opposed to the spherulitic or cryptocrystalline textures notable in spheres preserving primary textures.

Neomorphic recrystallisation is noted in sample C11 (Figure 4A), where recrystallisation has occurred in-situ within individual spherulitic crystals to reprecipitate larger interlocking crystals of siderite. Sample W1 contains wholly recrystallised spheres, with interlocking crystals (50–100 μm edges) that do not preserve any primary structure (Figure 4C), unlike the well-preserved

spheres (Figure 3A through D). By comparison, sample C12, stratigraphically 20 m below C11, records only partial recrystallisation of the core with interlocking crystals of 5–10 μm edges, whereas the outer rim preserves the primary spherulitic morphology (Figure 4B). Compositional heterogeneity within individual recrystallised spheres is prominently indicated by contrast changes in BSE images (element maps provided in Supplementary Information, Section 2.2.3). There is no evidence of secondary carbonate phases within the matrix from bulk samples analysed via XRD to suggest post depositional alteration within these palaeosol horizons containing recrystallised spheres.

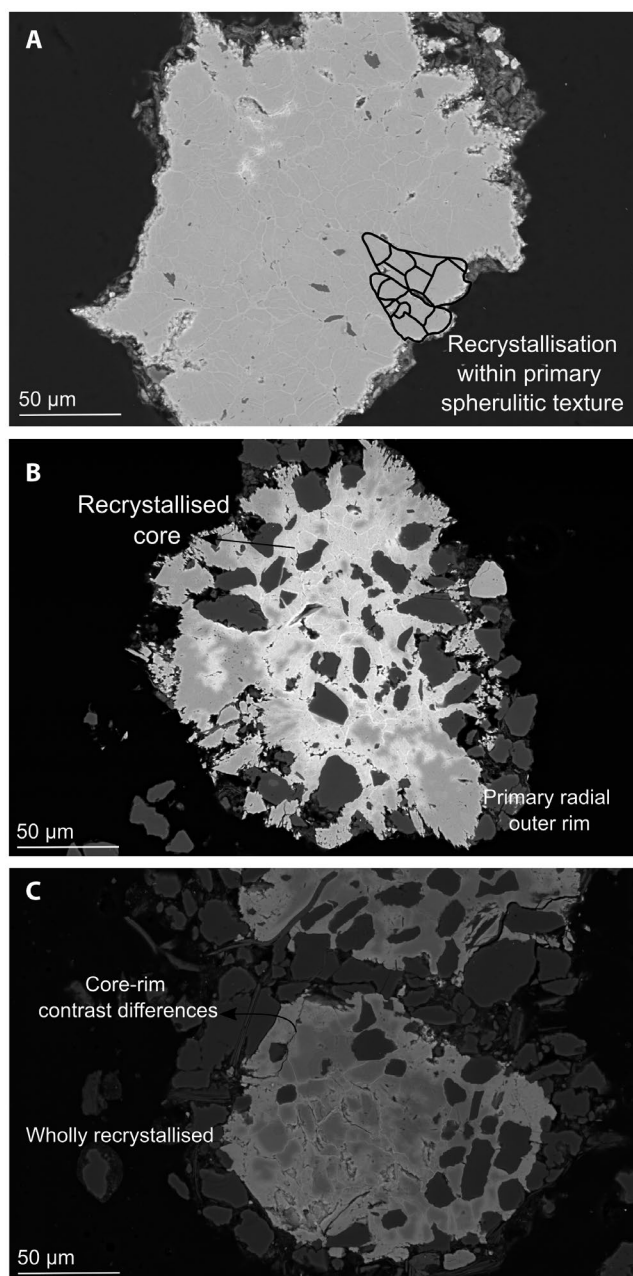


FIGURE 4 Recrystallisation in sphaerosiderites (A) C11, Wadhurst Clay, Cooden borehole where recrystallisation occurred within individual crystals, preserving original spherulite shapes. Example traced over on the right side of the sphaerosiderite to highlight this recrystallisation within a spherulite. (B) C12, Wadhurst Clay, Cooden borehole, where the core is recrystallised, but the rim preserves primary spherulitic texture. (C) W1, Wadhurst Clay, Westfield borehole, which is wholly recrystallised

3.1.3 | Dissolution textures

Examples of dissolution in sphaerosiderites (e.g. $<5\ \mu\text{m}$ diameter dissolved areas within a sphere) are notable in four horizons as concentric zones of dissolution or missing cores (Figure 5). These features are interpreted as a result

of finer crystal sizes and therefore shorter particle lifetimes upon dissolution. The host matrix for these spheres is similarly friable in DI water as other sphaerosiderite-bearing samples, and no other phases of carbonates are noted in the bulk matrix of these samples.

3.2 | The XRD of picked sphaerosiderites and bulk samples

Mineralogy within spheres varies from 1 to 100 wt% siderite, 13–89 wt% quartz, and 1–70 wt% clays (kaolinite and illite) (Figure 6). Anatase and pyrite were detected at low concentrations within the sphaerosiderites, at or below estimated quantification limits (*ca* 1–2 wt%). The sphaerosiderites from the Ashdown Formation appear to contain more kaolinite than those from the Tunbridge Wells Sand, but illite and quartz content varies to a similar extent within the formations (Figure 6). The XRD from bulk samples confirms that the matrix consists mainly of quartz, kaolinite and illite, with minor ($<3\ \text{wt}\%$) muscovite, consistent with thin section petrography. The dominant carbonate phase present in most of the sphaerosiderites is siderite, although the d-spacing of some diffraction peaks deviates from pure siderite due to substitutions of Mn, Ca and/or Mg (Supplementary Information, Section 2.1.2). In a few samples (e.g. CX4, C11), rhodochrosite was identified by XRD in addition to siderite.

3.3 | Element mapping and transects

3.3.1 | Mapping zones of minor element uptake

Elemental composition was characterised into types of patterns, based on variation across element maps and transects (e.g. changes in composition within zones, core to rim trends, whether there were angular blocks in a sphere) (Table 2). Representative examples of these patterns show that spheres from the same horizon generally fall into the same compositional type, but patterns vary between sphaerosiderite horizons (Figure 7), similar to the morphological patterns noted previously (See Supplementary Data for list of sphaerosiderite horizons).

Concentric zones of varying elemental composition are common in sphaerosiderites, and are divided into two categories; Compositional Type 2a (core-rim compositional change); such as Sample C9 (Figure 7) which contains higher concentrations of Mn (bright teal colour) in the core of the nodule and comparatively higher concentrations of Ca (blue) and Mg (green) in the outer rim, and Compositional Type 2b (multiple concentric zones of

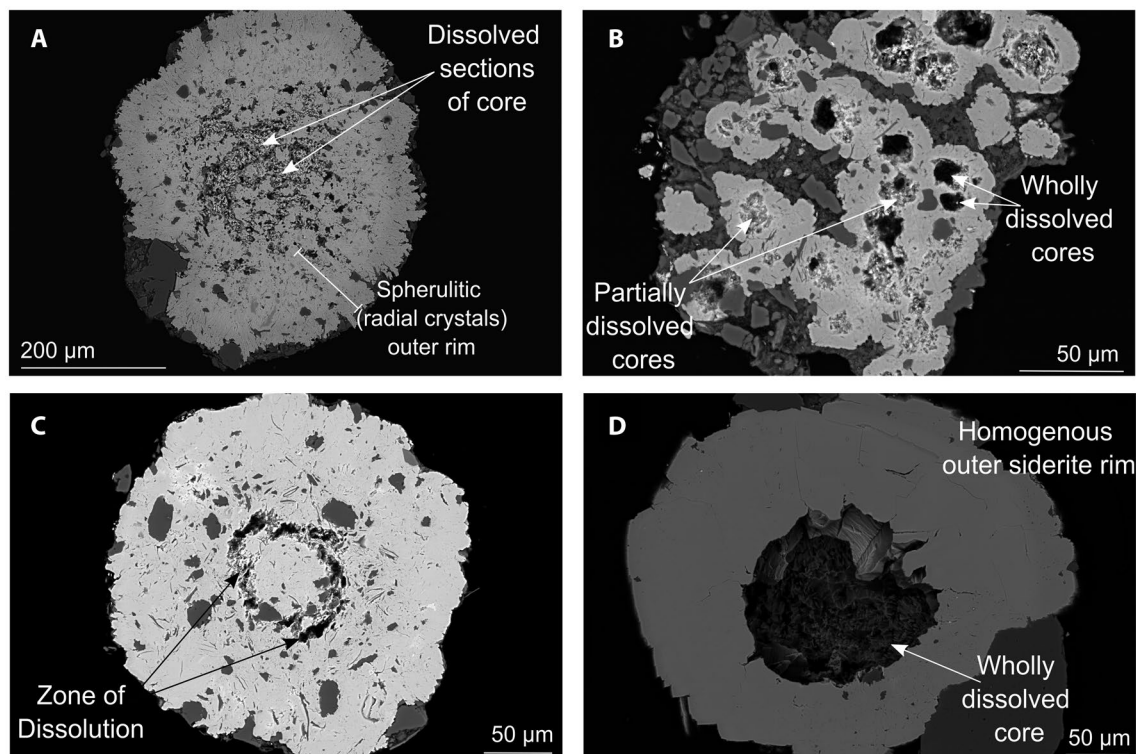


FIGURE 5 SEM BSE images displaying dissolution textures from a range of stratigraphic horizons within the Wealden Supergroup (A) FX6, Ashdown Formation (B) F19, Ashdown Formation, (C) CCX1, Tunbridge Wells Sand, and (D) CCX2, Tunbridge Wells Sand where the missing core was probably organic matter, which decomposed

varying composition and thickness); such as Sample C1 which shows greater Mn concentrations confined to a concentric zone within the sphere (Figure 7).

Differences in composition within spherulitic or angular zones (Compositional Type 2c) are notable in sample W2 (Figure 7), which is representative of spheres with a differentiated composition between crystal faces. In this sphere, there is an anti-correlation between Fe and Mn, and Fe and Ca, due to substitutions of Mn and Ca in the angular zone and in rims, while no significant correlation exists between Fe and Mg. Along with the differences in elemental composition in the angular blocks, fine ($<10\ \mu\text{m}$) concentric zones of higher Mn and Ca uptake are also notable in the edges of the sphere.

Lastly, some spheres do not show any discernible compositional patterns in EDS or EPMA and are compositionally homogenous; these spheres are classed as Compositional Type 2d (Example provided in Supplementary Information, Section 2.2.1).

3.3.2 | Quantitative elemental transects

The EPMA transects were conducted on a representative set of spheres from those used for SEM-EDS mapping. Transects support the compositional heterogeneity from

element maps and confirm that the majority of sphaerosiderites are pure FeCO_3 ($>90\ \text{mol.}\%$) (Data S1). The strength of correlations between cations (Fe, Ca, Mg, Mn), and concentrations of minor cations (Ca, Mg, Mn) are similar in spheres from the same horizon but vary between horizons, supporting the observations from element maps.

The transects also showcase the variety of relationships between minor cations, and hence the variability within compositional types. For example, a Compositional Type 2a (core-rim difference) sphaerosiderite may have an Mn enriched core, and a relatively Ca and Mg enriched rim (Figure 8), or vice versa (Supplementary Information, Section 2.2.2). Regardless, there is a strong negative correlation between Fe and the cations enriched in the core. Spheres with angular zones of enrichment (Compositional Type 2c) are also quantifiable in transects (Supplementary Information, Section 2.2.2), in most cases showing an enrichment of minor cations (Mn or Ca) within a spherulite relative to Fe.

Relationships between the minor cations are also variable between horizons (all data and correlation coefficients presented in Data S1). For example, both Mg and Ca are enriched in the rim of sample F6, and positively correlated ($R^2 = 0.625$), while in other horizons these elements may show no correlation (Figure 8).

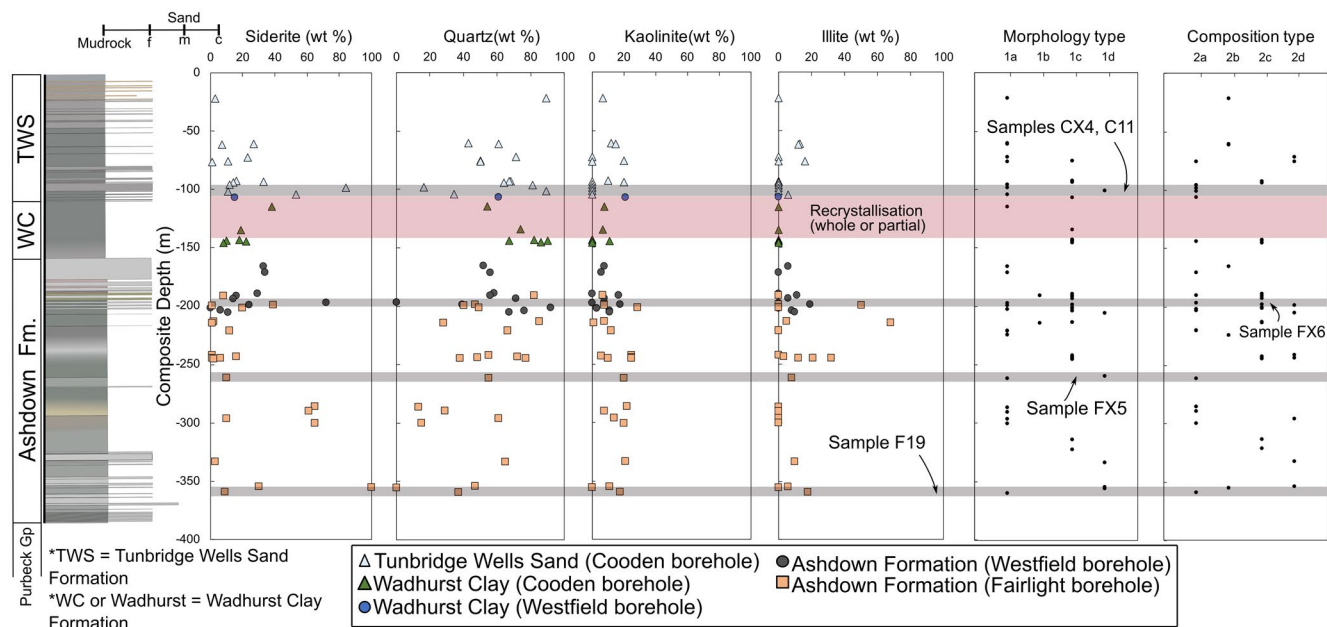


FIGURE 6 Mineralogy of picked sphaerosiderites, Morphology and Compositional types (see Sections 3.1.1 and 3.3.1 respectively) of spheres by composite depth. The composite log shows average grain sizes and lithology colour noted within the British Geological Survey log reports. Due to the close proximity of the Fairlight, Cooden and Westfield boreholes, it is assumed that each formation is time-correlative between boreholes. As these three boreholes each had a complete record of one of the three formations (see Figure 1), the composite depth was produced by assuming due to the proximity the sedimentation rate and thicknesses for each formation would be similar within the three boreholes. Tie points between boreholes were defined on lithostratigraphic correlation. Recrystallised sphaerosiderites are notable in all three boreholes within the Wadhurst Clay (highlighted in red). Depths of samples containing other carbonate minerals (see Section 3.4) alongside siderite are highlighted in grey; (1) Sample F19 contains calcite blocks, calcite-siderite interchanging layers with cores dissolved, (2) Sample FX5 contains calcite rhombs as inclusions and in matrix, and (3) Samples CX4 and C11 contain minor rhodochrosite (7–9 wt%) and dissolved cores. The Cuckfield samples were not included in this compilation as they were not analysed via XRD

TABLE 2 Description of compositional types within Wealden Sphaerosiderites

Composition type	Description	Variations
2a	Concentric zones: core-rim differences in uptake in a single sphere	Can be either Mn rich core and Mg and Ca rich outer rim, or vice-versa
2b	Multiple concentric zones of uptake in a single sphere	Usually increased Mn uptake in a concentric zone (of a range of diameter) but can also be Ca or Mg
2c	Spherulitic or Angular zones of uptake within a sphere	Usually enrichment of Ca, likely on a spherulitic crystal face
2d	Homogenous: elemental concentrations constant through the sphere	

The patterns of elemental distribution (compositional types: concentric zones, core-rim differences, angular spherulitic zones or homogenous) are variable between sphaerosiderite horizons and do not correlate with stratigraphic position, host lithology, or formations (Figures 6 and 9). This is reflected in the scattered data when all Fe versus minor cation concentrations are plotted for each formation (Figure 9), reflecting the variations in strength and relationships between cations of individual sphaerosiderite horizons.

3.4 | Growth relationships between siderite, pyrite and calcite within spheres

3.4.1 | Siderite and Pyrite

Elemental mapping of the large pyrite inclusions (discussed in Section 3.1.1) from the Ashdown Formation confirms the inclusions within the pyrite are mainly siderite, with occasional quartz and clays (Figure 10). The pyrites are primarily concentrated within an area <50 μm from the edge

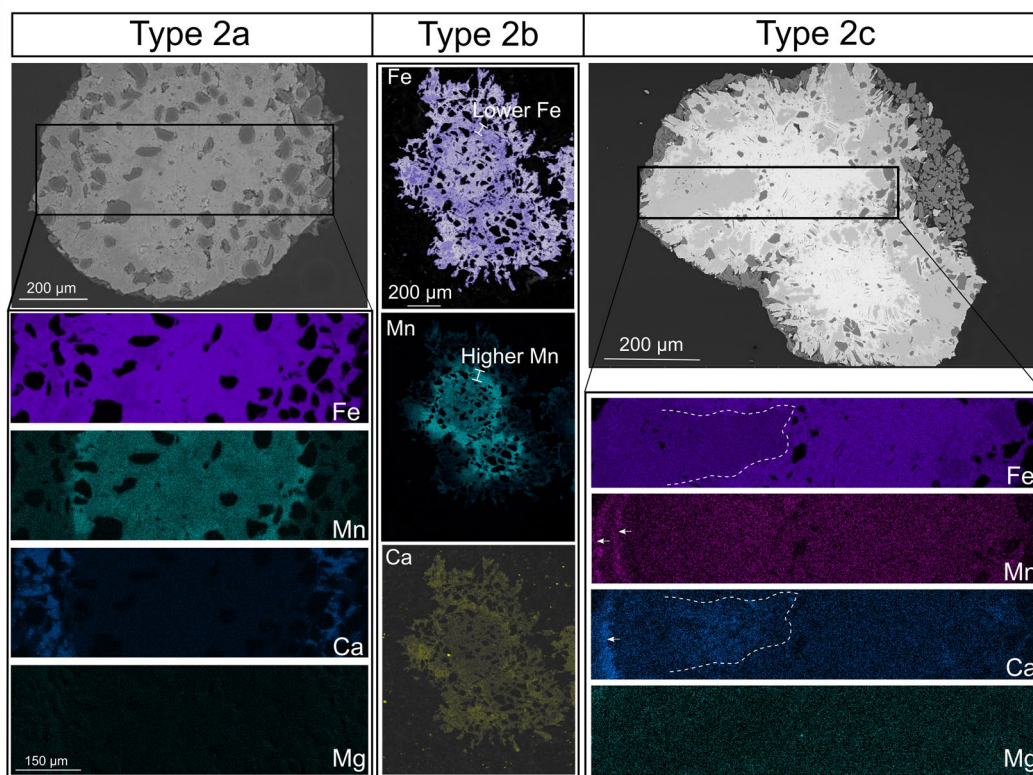


FIGURE 7 Representative samples of compositional Type 2a, 2b and 2c (Data from SEM BSE image and SEMEDS maps). Compositional Type 2a: Sample C9 (Tunbridge Wells Sand) contains spheres with a Mn rich core and a rim enriched comparatively in Ca and Mg. Compositional Type 2b: Sample C1 (Tunbridge Wells Sand) showing concentric zones of Fe and Mn enrichment, with Fe-Mn concentrations anti-correlated. This is a particularly oxidised sample (1:2 ratio of siderite to hematite) but preserves fine scale elemental variations in Fe and Mn concentrations. Compositional Type 2c: W2 (Ashdown Formation) showing evidence of spherulitic/angular parts of the nodule enriched in Ca corresponding to lower Fe content (less bright areas in Fe map—dotted white line)

of the sphaerosiderite corresponding to the darker contrast in the BSE image. Within the pyrite, the siderite inclusions are mainly concentrated in a central region, 5–10 μm in diameter, and are surrounded by an outer rim composed of blocky pyrite mostly devoid of inclusions.

3.4.2 | Multiple carbonate phases

The presence of calcite was noted in two sphaerosiderite horizons from SEM-EDS images and element maps, but calcite was not detected via XRD. The relationship between calcite and siderite in sphaerosiderites from sample F19 (Ashdown Formation) indicates that the sphere possesses a calcitic core and a siderite rim that are separated by a transition region in which both phases are present in alternating fine layers (<2 μm) (Figure 11). Although calcite is the dominant phase in this sphere, other spheres from this horizon are dominantly siderite with calcite incorporated as a minor phase, suggesting that the extent of calcite precipitation may have varied spatially within a single palaeosol horizon.

In contrast, the sample CCX2 (Figure 11) contains homogenous cryptocrystalline sphaerosiderites, all with a similar morphology and elemental chemistry, but with equant (1 μm edge length) inclusions of calcite rhombs within the sphaerosiderites and in the matrix. Within the sphere, the calcite rhombs are present in clusters of 6–12, dispersed primarily within 50–70 μm from the edge of the sphere, creating a mottled appearance in BSE images. On the edges of the sphere, the siderite can be seen growing around the calcite rhombs, implying the calcite rhombs were present in the matrix as the siderite sphere was growing and incorporating matrix phases.

3.5 | $\delta^{18}\text{O}_{\text{siderite}}$ and $\delta^{13}\text{C}_{\text{siderite}}$ of selected spheres

To evaluate whether compositional and morphological heterogeneity is also associated with changes in isotopic composition, three samples previously reported in Robinson et al. (2010), FC5, FC9 and FC11, were analysed using SIMS.

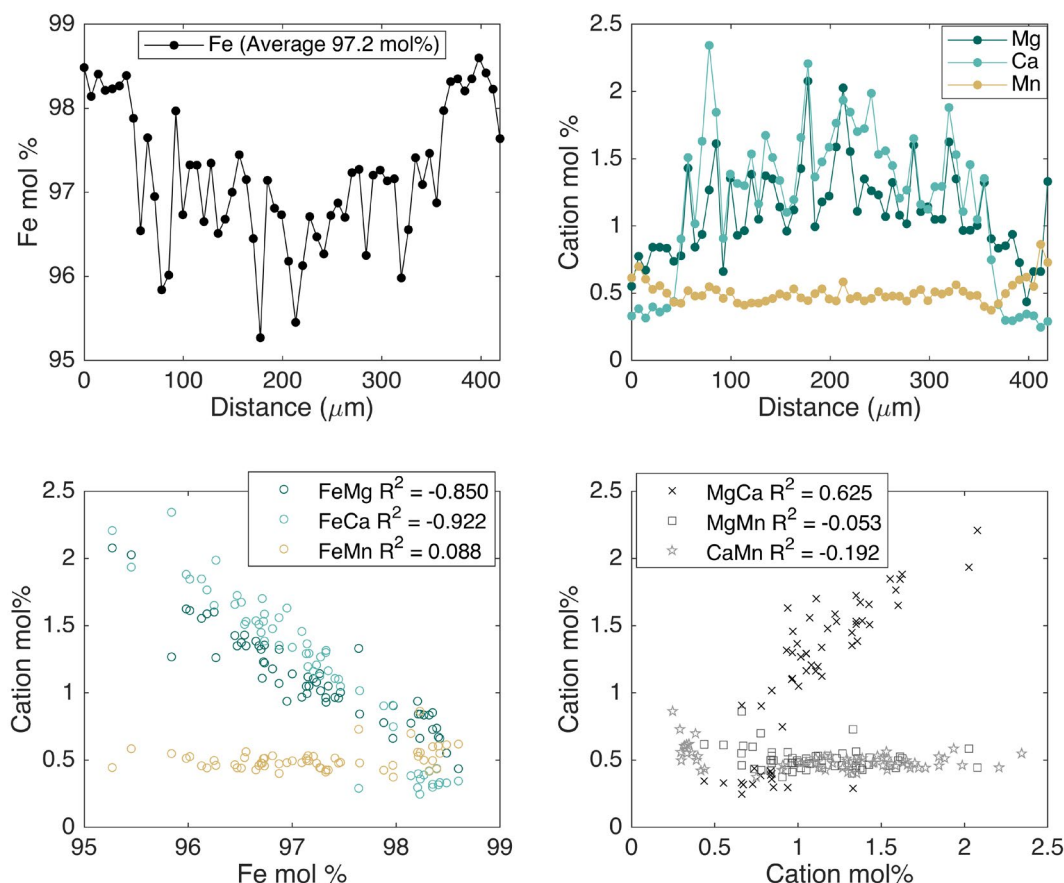


FIGURE 8 Elemental transect (using EPMA) from F6 (Ashdown Formation), showing higher concentration of Ca and Mg in core, negatively correlated to Fe. Mn concentrations remain low throughout the transect. Other variations of elemental uptake patterns can be found in Supplementary Information Section 2.2.2

The $\delta^{13}\text{C}_{\text{siderite}}$ transects generated by SIMS show a common pattern amongst all spheres analysed; a core with relatively isotopically light $\delta^{13}\text{C}_{\text{siderite}}$ (-20‰ to -35‰), and a gradual trend to isotopically heavier values towards the rim (-1‰ to -10‰) (Figure 12, Supplementary Information Section 2.4). The $\delta^{13}\text{C}_{\text{siderite}}$ measured values are consistent with values expected from soil processes, including methanotrophy (Ludvigson et al., 1998). The $\delta^{18}\text{O}_{\text{siderite}}$ transects also show a general pattern in some spheres, with values decreasing from core to rim by up to 3‰ . This trend of $\delta^{18}\text{O}_{\text{siderite}}$ from core to rim is seen clearly in FC9 and FC5 (Supplementary Information, Section 2.4) but is less clear in FC11 (Figure 12). These trends in $\delta^{18}\text{O}_{\text{siderite}}$ could potentially be explained by elemental heterogeneity in the sphaerosiderites. Spheres of FC5 and FC9 are on average $>90\text{ mol.}\%$ siderite, but increased concentrations of Mg (3–10 mol.%) and Ca (1–4 mol.%) are present at points on the rims (Supplementary Information, Section 2.4). Changes in elemental concentration can lead to uncertainties when correcting $\delta^{18}\text{O}_{\text{siderite}}$ values measured by SIMS (Rollion-Bard & Marin-Carbonne, 2011) and so the decrease in values towards the rim may be an artefact of this. This suggested

analytical artefact is further supported by elemental and isotopic transects of sample FC11, where Mg and Ca enrichment varies more erratically over the sphere (Figure 12), and the $\delta^{18}\text{O}_{\text{siderite}}$ transect is noisy compared to FC9 or FC5 where Mg and Ca enrichment is more consistent across the sphere. This methodological issue also means that the SIMS stable-isotope values reported here are not directly comparable with conventional measurements of siderite $\delta^{18}\text{O}$ by gas source isotope ratio mass spectrometry.

4 | DISCUSSION

4.1 | Variable physiochemical conditions during the growth of Wealden sphaerosiderites

4.1.1 | Morphological, compositional and isotopic heterogeneity

Morphological changes, at a basic level, can be used to understand changes in relative saturation states with respect

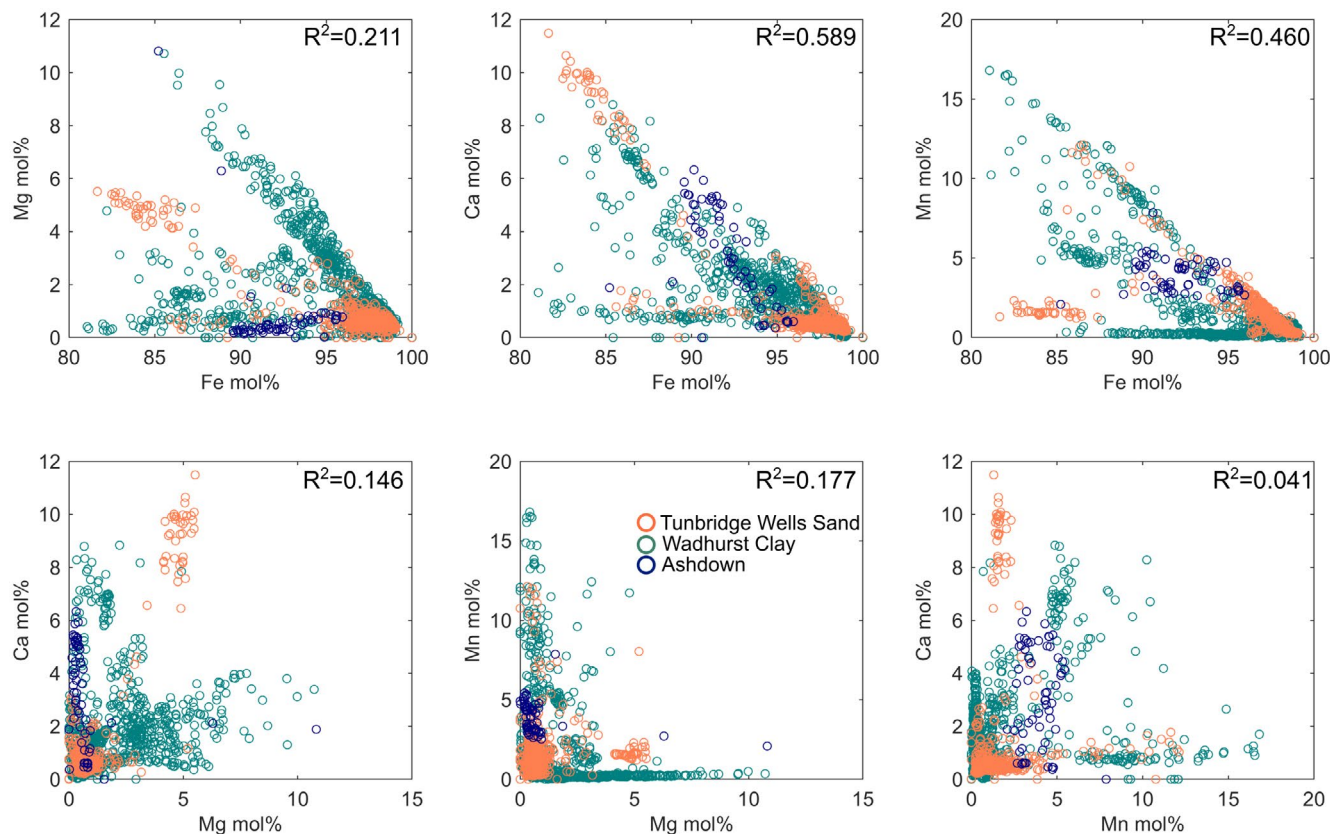


FIGURE 9 Correlations between all elemental transect data shows a large scatter. None of the correlations are statistically significant, apart from between Fe and Ca. These data comprise analyses of 19 spheres from the Ashdown Formation, two from the Wadhurst Clay Formation, and eight from the Tunbridge Wells Sand Formation. Graphs for individual formations are available in Supplementary Information Section 2.2.2

to siderite. For instance, the cryptocrystalline centre of spheres probably formed during a period of high siderite nucleation rate, which would be triggered by locally high supersaturation above a key threshold (Passey, 2014). As siderite precipitated and saturation state decreased, nucleation rates decreased correspondingly, and continued crystal growth was favoured. This scenario may explain, for example, the formation of outward-radiating bladed/spherulitic crystals, whereby supersaturation remained poised below the critical threshold for spontaneous nucleation but high enough to permit rapid spherulitic growth (Passey, 2014). Although this mechanism may apply to some examples (e.g. Figure 3), morphologies within many of the Wealden sphaerosiderites are far more diverse. The spheres include evidence of cryptocrystalline centres with spherulitic rims, but also wholly cryptocrystalline spheres, spheres with several growth zones indicating multiple periods of growth, and irregular morphological changes within individual spheres. The variety of morphologies between different stratigraphic horizons, combined with the similarity of morphologies in spheres from the same horizon, indicates growth rate differences linked

to temporal variability in the siderite saturation state of local pore waters controlled by pH, temperature, Fe^{2+} concentration, and total dissolved inorganic carbon (DIC). As with morphological changes, compositional changes within individual sphaerosiderites also show a great deal of variability. The patterns of minor element (i.e. Mn, Ca and Mg) distribution in the Wealden sphaerosiderites are similar in spheres from the same stratigraphic horizon, but vary between horizons, and this variability appears decoupled from lithological or facies changes (Figure 6), suggesting local controls on morphology and element chemistry.

Multiple geochemical controls on the chemical composition of siderite can complicate palaeoenvironmental interpretations of elemental composition (Mortimer et al., 1997; Romanek et al., 2009; Sengupta et al., 2020). For instance, higher concentrations of Mn compared to Ca or Mg have been used to suggest sphaerosiderite growth in freshwater (Mozley, 1989), and Wealden sphaerosiderites, indeed, commonly contain Mn as a minor element (Figure 7; Robinson et al., 2010). Recently, however, Mn incorporation into growing

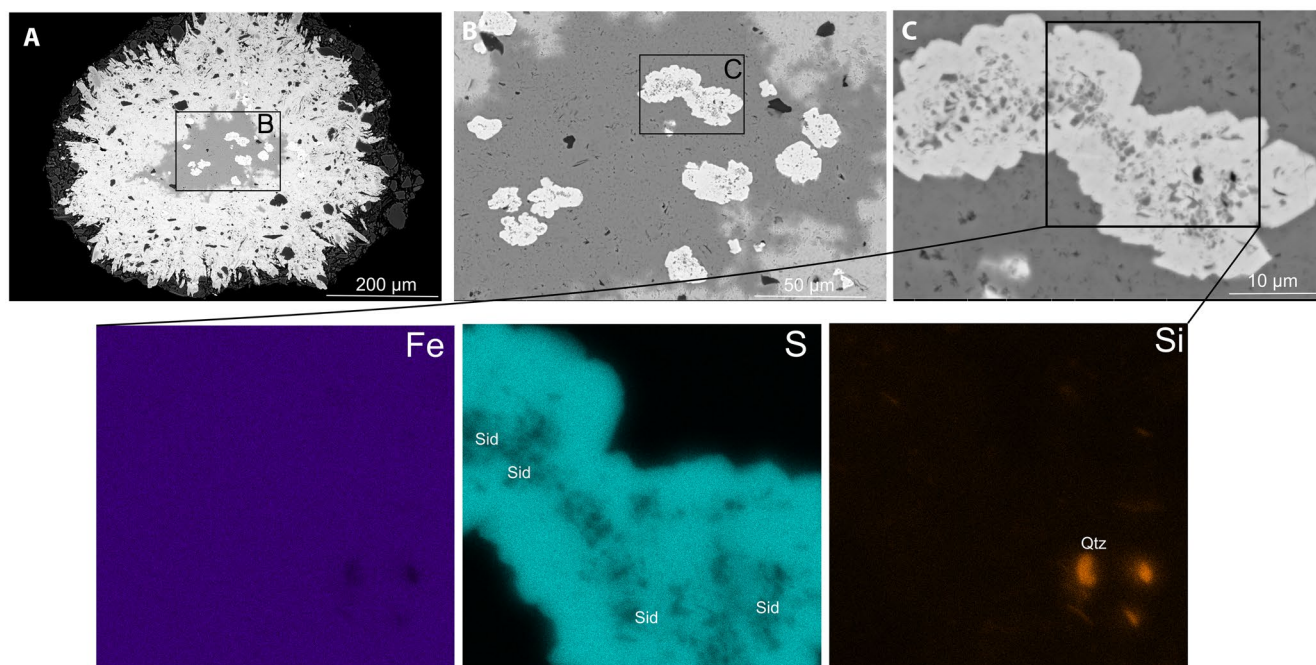


FIGURE 10 (A) BSE image of a sphaerosiderite from Sample F10 (Ashdown Formation), (B) BSE image of central section of the same sphaerosiderite, and (C) BSE image of a pyrite inclusion within the same sphaerosiderite and SEM-EDS maps of the pyrite inclusion and surrounding matrix. The pyrite inclusions are rounded with blocky edges, randomly orientated, and dispersed through the core of the sphere. The pyrite inclusions contain siderite inclusions within, and minor quartz and clays

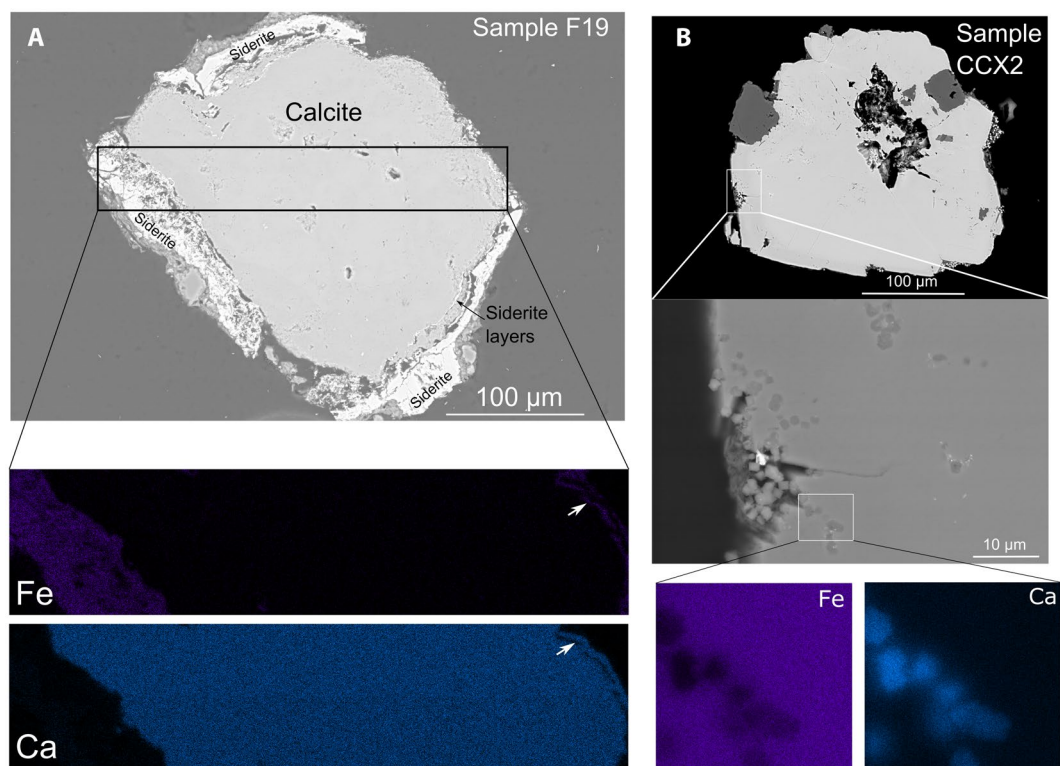


FIGURE 11 BSE images and SEM-EDS maps displaying (A) Sample F19 (Ashdown Formation) contains a pseudo sphaerosiderite, consisting of a calcite block with siderite growing on the rim and layers of intergrowth in between, and (B) Sample CCX2 from the Tunbridge Wells Sand, a siderite sphere with a cryptocrystalline centre and calcite rhombs growing in the matrix surrounding the spheres, and incorporated into the sphere. The core of the sphere is partially missing, and probably organic matter that decomposed

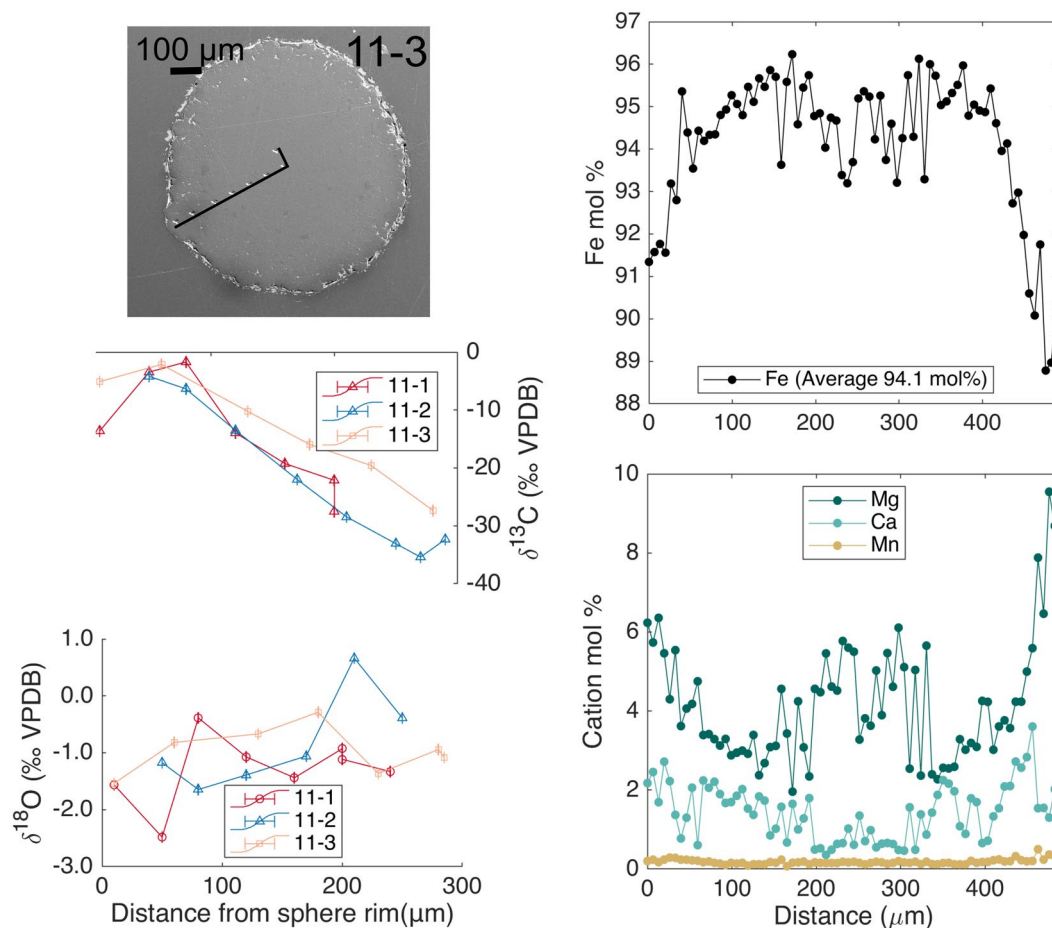


FIGURE 12 Stable isotopes ($\delta^{13}\text{C}$, $\delta^{18}\text{O}$) of three spheres from Sample FC11 (sample details originally reported in Robinson et al. 2010) showing patterns in carbon and oxygen isotopes across transects. The carbon isotopes decrease from rim to core, while oxygen isotopes increase from rim to core, but the oxygen isotope transects are noisier. A representative elemental transect from FC11 shows variability in minor element compositions through the sphere, that are likely to affect the correction factors applied to oxygen isotopes in SIMS

siderite has been shown to be controlled by both the concentration of Mn in solution and the growth rate (Sengupta et al., 2020). It is not possible to distinguish between the influence of growth rate and cation concentration in sphaerosiderites examined here; Mn uptake is not usually accompanied by coincident morphological changes. Similarly, Mg or Ca enrichment, compared to Mn, has been suggested to indicate the presence of marine pore waters (Mozley, 1989). In the Wealden Supergroup, there is no stratigraphic pattern in the correlations between Fe and Ca or Fe and Mg (Figure 9), probably due to the range of spatial element patterns within spheres (e.g. core or rims can be enriched in Mn, Mg or Ca) and the absence of a consistent degree of statistical correlation between these elements (Figure 9). The enrichments of Mg and Ca in sphaerosiderite cores is unusual, especially in light of laboratory synthesis studies which show that Mg and Ca uptake into siderite is negligible at room temperature (Romanek et al., 2009; Sengupta et al., 2020), and such chemical

features may be more consistent with diagenetic reactions (such as recrystallisation at higher burial temperatures). Importantly, a lack of secondary cements such as ferroan carbonates, and a lack of alteration in most of the sphaerosiderite horizons (apart from the limited horizons identified with dissolution or recrystallisation; Figure 6) suggests that the Wealden sphaerosiderites preserve primary morphology and composition, and that the elemental heterogeneities probably reflect the chemical conditions surrounding siderite growth shortly after sediments were deposited.

In the limited number of spheres analysed via SIMS, it is clear that along with morphological and compositional heterogeneity, they preserve an isotopically heterogeneous signature. As discussed previously, the oxygen isotope heterogeneity in transects may in part be due to difficulties with matrix corrections in siderite and the relative change cannot be reliably interpreted; however, this potentially heterogeneous isotopic composition could indicate a complex palaeohydrological record and

should be investigated further. The trend in $\delta^{13}\text{C}_{\text{siderite}}$ across spheres should be unaffected by matrix heterogeneities (Rollion-Bard & Marin-Carbonne, 2011). Heavier $\delta^{13}\text{C}_{\text{siderite}}$ values (up to 5‰) at the rim compared to the core could suggest variability in the water table, resulting in changes to the depth of the zone of methanogenesis, that would have created an isotopically-heavy pore water DIC pool (Ludvigson et al., 1998). This would imply that the palaeohydrology recorded by the sphaerosiderites over time changed and that the carbon isotopes are reflecting fluctuations in the depth of boundaries between respiration pathways in the soil zone during growth. It is difficult to quantify depths from isotopic studies as the depths at which methanogenesis would operate may be spatially (and temporally) variant (Ludvigson et al., 1998, 2013).

4.1.2 | Depth of sphaerosiderite growth

Understanding the depth at which sphaerosiderites were growing is paramount to understanding the extent to which surface processes may have affected them and how best to interpret palaeoclimate signals recorded by them. For instance, studies on modern systems have shown that siderite nodules typically grow just below the water table, from 1 to 2 m below the soil surface (Driese et al., 2010; Pye et al., 1990; Van Dijk et al., 2019). It has also been suggested that modern nodules growing deeper within a soil profile appear to record less seasonality, based on clumped isotope temperature measurements (Fernandez et al., 2014; Van Dijk et al., 2019). The morphological and elemental heterogeneity recorded within individual Wealden sphaerosiderites are interpreted as changes in physiochemical conditions during growth and could indicate growth relatively close to the soil surface, where conditions are probably to have been more dynamic. The pore waters can be variable within a wetland and regularly experience changes in groundwater chemistry, such as pH, temperature, cation concentrations and/or soil pCO_2 , all affecting siderite growth (Driese et al., 2010; Lin et al., 2019; Ludvigson et al., 2013; Mitsch et al., 2010). Sphaerosiderites in the Weald Basin have also been associated with root structures (Allen et al., 1998), providing further evidence that they grew at relatively shallow depths in the soil profile, and were probably affected by surface processes. Assessing the depth of the Wealden root systems is difficult, but coupled with the morphological and elemental heterogeneity, and the lack of extensive diagenetic alteration or cements, it can be argued the Wealden sphaerosiderites were recording meteoric groundwater but were growing at depths within the soil profile where pore waters experienced physiochemical variability during growth.

4.1.3 | Origin of pyrite inclusions in sphaerosiderites

The formation of pyrite relies on the presence of iron, the availability of dissolved SO_4^{2-} , and the amount of organic matter that can be used by sulphate reducing bacteria to produce H_2S (Berner, 1971). In the presence of sufficient sulphate, ferrous iron would be expected to react with H_2S rapidly, largely precluding a siderite precipitation pathway (Berner, 1983; Pye et al., 1990). Based on the high concentrations of siderite in the Wealden Supergroup, it is inferred that Fe^{2+} was in abundance relative to sulphide during growth. Pyrite, present as inclusions within sphaerosiderites in low (<1 wt%) concentrations (horizons highlighted in Data S1), probably formed from the consumption of low concentrations of initial sulphate and was potentially restricted to areas of locally dispersed organic matter.

In two sphaerosiderite horizons, sphaerosiderites contain pyrite inclusions with diameters >20 μm , and the pyrite inclusions themselves contain siderite inclusions. This suggests that local conditions within the wetland were fluctuating between sulphide and carbonate precipitation, potentially related to micro-scale sulphate variations, controlled by diffusion between the zone of sulphate reduction and siderite precipitation (Lin et al., 2019 and references therein). The petrographic relationships suggest that initially small siderites (<5 μm length) precipitated in siderite-saturated pores filled with freshwater, but then conditions switched to those favourable for pyrite precipitation, at least at the micron scale (Figure 13). The pyrite growth incorporated existing small siderites into a cryptocrystalline centre, before slower growth rates produced a blocky cubic rim. The fact that the siderite inclusions are mostly incorporated in the central region of the pyrite spheres suggests that pyrite was growing in the same locations as siderite. Over time, however, the pore waters became dominantly siderite saturated, presumably once the low sulphate concentrations were exhausted (Figure 13).

4.1.4 | Minor calcite precipitation

Similar to the pyrite–siderite petrographic relationship, the siderite–calcite relationship suggests locally fluctuating and spatially variant conditions between calcite and siderite precipitation. Evidence includes some calcite–siderite co-existence (Figures 6 and 11) within the Wealden sphaerosiderites, where calcite is noted both as a dominant component in some spheres within a horizon (F19), and as a minor component as inclusions within spheres (CCX2). At the same saturation state, calcite is known to grow up to seven orders of magnitude faster than siderite

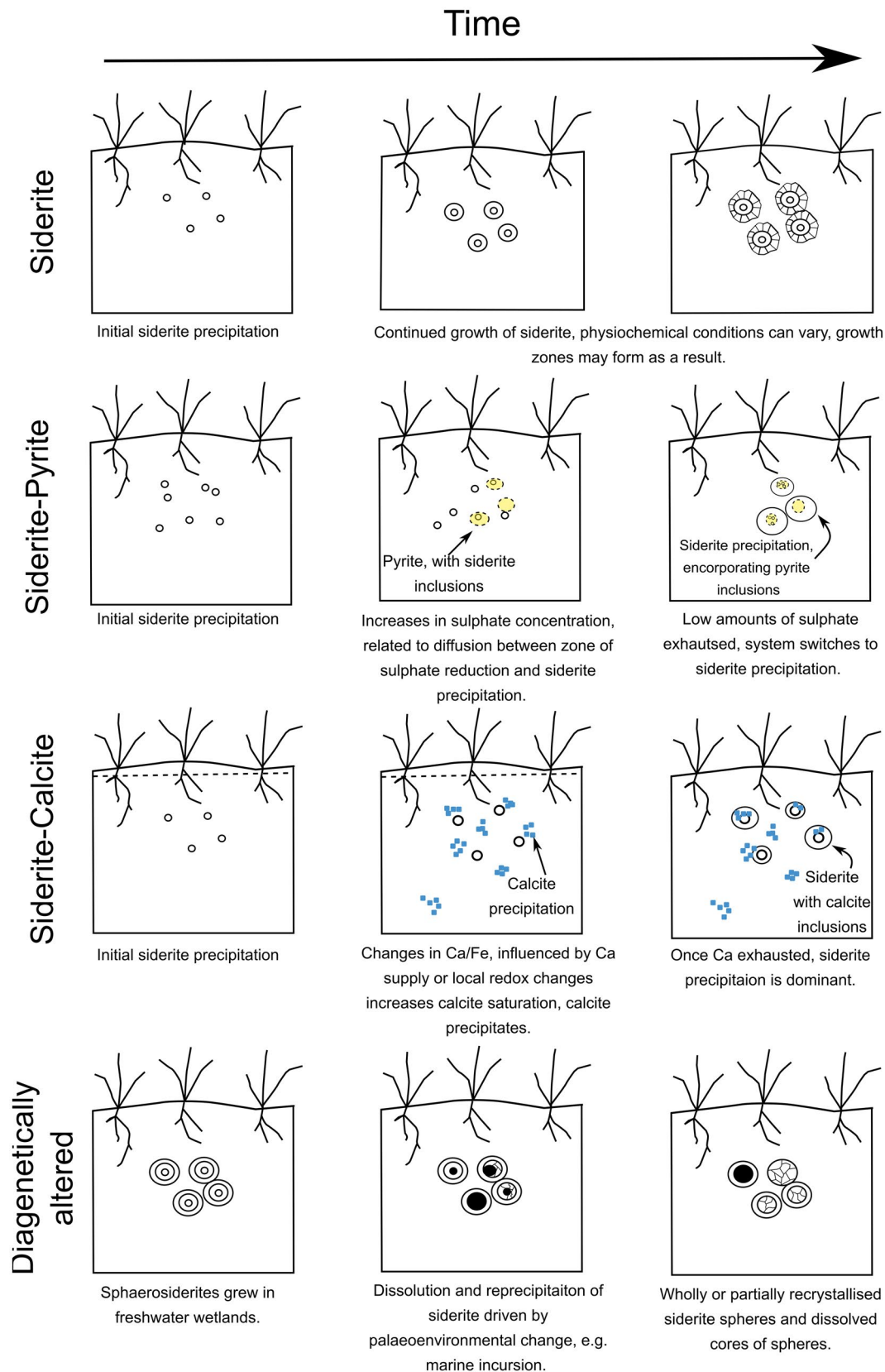


FIGURE 13 Schematic summarising the formation processes of the Wealden sphaerosiderites

(Busenberg et al., 1986; Jiang & Tosca, 2020). This means that even at very low concentrations of Ca (1/100th of Fe), calcite growth would still be dominant (Jiang & Tosca,

2020). The presence of calcite as a locally dominant component, and within transition layers interspersed by siderite layers indicates that overall, Ca was probably low in

the Wealden wetlands, and calcite precipitation was probably a response to fluctuating Ca and variations in anoxia, which, together would influence the Ca/Fe ratio of pore water (Figure 13). However, the prevalence of sphaerosiderites in most horizons suggests that the soils were more commonly Ca-limited relative to Fe and featured persistently reducing environments that established siderite as the dominant carbonate precipitation pathway.

4.2 | The Wealden palaeoenvironment

4.2.1 | A dynamic palaeoenvironment

Modern wetlands are highly variable and dynamic environments and major components of a wetland hydrological system include the amount and timing of precipitation and evaporation, surface inflows and outflows, and groundwater fluxes. Together these all influence physiochemical conditions such as soil chemistry, water chemistry and sediment composition (Mitsch & Gosselink, 2015). Siderites growing in modern wetlands have been shown to record a seasonal bias in temperature (Van Dijk et al., 2019), and are associated with variable groundwater $\delta^{18}\text{O}$ (Driese et al., 2010; Ludvigson et al., 2013), variable dissolved ion compositions (Lin et al., 2018; Moore et al., 1992; Pye, 1984; Pye et al., 1990) and variability in biological processes such as sulphate and ferrous iron reduction (Coleman et al., 1993; Lin et al., 2019).

It is reasonable to assume that ancient wetlands would have experienced similarly dynamic environmental conditions. Indeed, sedimentological evidence from the Wealden Supergroup across southern England suggests variable palaeohydrological conditions, with evidence for intervals of wet and dry conditions. Debris beds, storm coquinas and coarse channel deposits are thought to reflect storms and high channel discharge events (Allen et al., 1998; Wright et al., 2000), whereas the presence of groundwater laterites, calcretes and red vertisols suggests periods of drier, more arid conditions in some regions (Allen et al., 1998; Robinson et al., 2002; Wright et al., 2000). Periodic groundwater recharging associated with the wet climate conditions would have influenced cation concentrations, pH, and pCO_2 in pore waters, all of which would have affected siderite growth rates, morphology and elemental composition. Thus, the sedimentological evidence for changes in palaeohydrology lends support to the interpretations of variable physiochemical conditions in pore waters during sphaerosiderite growth based on the Wealden sphaerosiderite elemental and morphological heterogeneity.

Seasonal changes in the Wealden Supergroup are also interpreted from sedimentological evidence and climate models. Features indicative of seasonality include seasonal

catenas and rapidly deposited storm coquinas (Allen et al., 1998; Wright et al., 2000), and wood growth rings (Watson & Alvin, 1996). Climate modelling of the Wealden at four times pre-industrial levels of atmospheric CO_2 (ca 1,120 ppm) suggests hot summers (average land temperature 30–36°C) and cool winters (8–12°C), as well as precipitation throughout the year, with highest precipitation during winter months (Haywood et al., 2004). The sedimentological evidence for wet and warm conditions agrees with the climate model simulations of Haywood et al. (2004) relatively well, and suggest that the chemical variability observed in modern wetlands would probably have applied within the Weald Basin wetlands.

These wet and warm conditions in the Weald Basin during the Lower Cretaceous, varying on seasonal to much-longer timescales, would have been a major factor in controlling surface water flow and groundwater recharging, and therefore, the dynamics of the palaeoenvironment (Allen et al., 1998; Haywood et al., 2004; Watson & Alvin, 1996; Wright et al., 2000). For instance, the timing and amount of seasonal precipitation would control the timing of groundwater recharging and therefore, the geochemical stability of pore waters, having a direct influence on siderite growth. The continued growth of sphaerosiderites suggests the soils remained largely waterlogged for the duration of sphaerosiderite formation (potentially on the order of 100 years; Driese et al., 2010), but that they were probably growing high enough in the soil profile for the surrounding pore waters to be affected by seasonal surface changes and groundwater recharging.

4.2.2 | Brackish or marine influence in a freshwater wetland?

Modern nodules from intertidal coastal wetlands in Norfolk, UK (Lin et al., 2019; Pye, 1984; Pye et al., 1990) and the Mississippi River delta (Moore et al., 1992) contain multiple phases such as siderite, calcite, dolomite and pyrite, within the same nodule. The presence of Mg-calcite and pyrite in these modern systems was explained due to marine incursions in the wetlands and proximity to the coast (within 2–5 km). The proximity to the coast probably provides more sulphate and higher concentrations of Ca^{2+} and Mg^{2+} within pore waters leading to precipitation of pyrite and calcite (Moore et al., 1992; Pye et al., 1990).

Similar to these modern coastal wetlands, it is possible that marine influence in ancient wetlands may have allowed the growth of multiple phases such as siderite, calcite and pyrite. In the Wealden sphaerosiderites, pyrite is a common, but very minor, inclusion (<1 wt%) that probably formed prior to the exhaustion of low sulphate availability (Figure 10). By contrast, calcite precipitation may have been locally dominant compared

to siderite within certain horizons (Figure 6). At these times of dominant calcite precipitation, one possibility is that the pore water chemistry in the Wealden could have been influenced by marine/brackish sources to allow co-precipitation of multiple carbonate phases (as seen in the modern; Moore et al., 1992; Pye et al., 1990). Another possibility is that over time, the primary Mg-calcite, precipitating alongside siderite, could have recrystallised to Mg-rich siderite, a process observed in studies of late Holocene siderites from Norfolk (UK) over timescales <1,500 years (Lin et al., 2019; Pye et al., 1990). However, there is no obvious textural evidence of areas with high Mg contents within the Wealden sphaerosiderites that would suggest the presence of originally Mg-calcite. The Mg content within spheres from the Wealden is generally relatively low, and therefore the presence of other carbonate phases within the nodules, such as calcite, are stronger, less ambiguous evidence for brackish pore waters than Mg concentration alone.

The recrystallisation of sphaerosiderites in the Wadhurst Clay in multiple boreholes (Figure 6) is evidence of regional stratigraphic alteration which could also suggest widespread palaeoenvironmental changes (Figure 13), such as a marine incursion. Similar recrystallisation of sphaerosiderites has been reported from the Cretaceous-age Dakota and Swan River formations in the western USA (Ufnar et al., 2004b) and linked to local sea-level changes due to the proximity of palaeocoastlines to the sampled sites (<10 km). In contrast, the Wadhurst Clay Formation sampled from the cores studied here would have been deposited >100 km from the Boreal Sea (Radley & Allen, 2012) and lacks other evidence of marine diagenesis (e.g. replacement of siderite by pyrite, calcite cements). Palynological and fossil assemblages provide inconclusive evidence of salinity fluctuations during deposition of the Wadhurst Clay (Batten, 1982; Batten & Lister, 1988; Horne, 1995), although the formation has been interpreted as a more oxidized and more transgressive facies than the formations above or below (Allen et al., 1998; Batten, 1982, 1998).

Based on mineralogical and petrographic evidence, the Wealden Supergroup may have experienced some periods of more brackish conditions but these do not seem to have been pervasive as there is no evidence of extensive pyrite or calcite deposition, and the sedimentological, petrographic and palaeontological evidence for higher salinities is inconclusive. For the most part, the palaeosol horizons within the Ashdown Formation and Tunbridge Wells Formation were probably growing in freshwater conditions and are suitable for palaeoclimate reconstruction by, for example, stable oxygen isotopes (Robinson et al., 2010). The regional recrystallisation in sphaerosiderites from the Wadhurst Clay suggests a significant palaeoenvironmental change; further work is required to understand the context and cause of this as

current palaeontological, sedimentological and palynological evidence is inconclusive.

4.3 | Sphaerosiderites as an accessible record of wetland geochemistry through the Phanerozoic

Throughout the Phanerozoic, sphaerosiderites preserve a variety of patterns in minor element uptake and morphologies similar to those noted in the Wealden Basin, including but not limited to, Mn-rich core, Mg and/or Ca-rich rim, Ca and/or Mn concentrations in certain radial zones within a sphere, and relatively constant minor cation concentration throughout the spheres (Choi et al., 2003; Driese et al., 2010; Khim et al., 2000; Passey, 2014; Ufnar et al., 2004b; Weibel et al., 2016). The preservation of such morphologies and elemental compositions have also been noted in the geological record older than the Phanerozoic (Bojanowski et al. 2020), and further work on pre-Phanerozoic sphaerosiderites would be key for comparisons to the more extensively documented Phanerozoic pedogenic siderite record.

As evaluated in the Wealden sphaerosiderites and supported by recent experimental work, the elemental heterogeneity within a single sphaerosiderite probably reflects a mixture of pH, saturation state, DIC, temperature and cation concentrations experienced during the growth of the sphere (Sengupta et al., 2020). Some of the Phanerozoic sphaerosiderite compositions have been attributed to palaeoenvironmental changes and groundwater chemistry (Ufnar et al., 2004b; Weibel et al., 2016), however, most studies have not usually provided comparisons between multiple microanalytical methods (e.g. thin section petrography, XRD, SEM, EDS, EPMA, SIMS), sedimentology, palynology, palaeontology and climate modelling to allow a more holistic understanding of palaeoenvironments (Choi et al., 2003; Coleman, 1993; Fisher et al., 1998; Kantorowicz, 1985; Khim et al., 2000; Mozley, 1989; Mozley & Carothers, 1992). The similarities in the range of morphologies and compositions recorded by Phanerozoic sphaerosiderites suggests they may have been recording dynamic wetland conditions and are an untapped resource for understanding terrestrial wetland dynamics in deep time.

The complexity of siderite growth in wetland systems is documented in modern nodules (Lin et al., 2019; Moore et al., 1992; Pye et al., 1990). The evidence from such studies suggests that precipitation of both calcite and siderite is common in these modern coastal settings, as is the presence of pyrite. All three of these phases are also notable in ancient wetland deposits (Fisher et al., 1998; Kantorowicz, 1985; Ufnar et al., 2004b; Weibel et al., 2016), suggesting a strong link between the deposition of these phases, and their preservation in the geological record. Both Lin

et al. (2019) and Pye et al. (1990) conclude that recrystallisation of calcite to siderite occurs within the modern nodules from Norfolk, providing another pathway to carbonate mineral formation other than direct precipitation. Lin et al. (2019) found that some localities in the Norfolk marshes contained pore waters with $\text{Fe/Ca} > 0.2$ (required for recrystallisation of calcite to siderite), but not others. This suggests that conditions may have been equally variable within ancient wetlands, allowing for recrystallisation processes to be operating locally based on cation concentrations in pore waters. The modern studies illustrate that, within the same wetland system, there are not only complexities regarding the palaeoenvironmental conditions (i.e. pH, cation concentration, saturation), but also regarding the pathway through which siderite can precipitate.

The mineralogical composition of Phanerozoic sphaerosiderites also indicates that similar pathways operated in ancient wetlands. The co-existence of siderite and pyrite within nodules has been previously noted in Triassic and Jurassic samples (Fisher et al., 1998; Kantorowicz, 1985), but unexplored. Calcite and siderite have also been found together in ancient wetland deposits (Kantorowicz, 1985; Ufnar et al., 2004b; Weibel et al., 2016), and may reflect fluctuations of sources of brackish and marine water, instead of those interpretations being solely attributed to siderite composition.

The presence of pyrite and calcite in sphaerosiderites from modern and ancient wetlands suggests a commonality in biogeochemical processes within wetlands through the Phanerozoic which needs to be explored and considered more in deep-time palaeoenvironmental reconstructions. It is therefore important for sphaerosiderite studies to consider the complexities that may have been present within ancient wetlands by thoroughly assessing mineralogy and petrography of the sphaerosiderites, and contextualising these data alongside sedimentological interpretations and recent constraints on siderite growth (Jiang & Tosca, 2020; Sengupta et al., 2020). Relying only on the elemental variations within a concretion does not necessarily provide the broad understanding of how an ancient wetland system was operating at the time of deposition and siderite growth. An approach covering multiple aspects such as petrography, elemental composition, mineralogy and sedimentology is likely to provide new insights into natural variability within ancient wetlands, and into important dynamic palaeoenvironmental conditions that probably existed in wetlands through the Phanerozoic.

5 | CONCLUSIONS

Sphaerosiderites are a complex palaeoenvironmental recorder but provide a useful tool for understanding ancient

palaeoenvironmental and palaeoclimate changes. The Lower Cretaceous Wealden Supergroup of southern England contains multiple well-preserved sphaerosiderite horizons which show a variety of morphologies and elemental compositions. Importantly, the morphology, elemental composition and pattern of element uptake within sphaerosiderites from the same horizons are similar, suggesting the textural and elemental changes recorded are influenced by the evolution of pore waters within that horizon. Wealden Sphaerosiderites are predominantly >90 mol.% siderite, but enrichments of Mn, Mg and Ca can range from 0 to 15 mol.% in individual points on transects, and on average up to 5 mol.% across spheres. Generally, the substitutions cause a negative correlation between Fe and the minor cations, but this is not always straightforward to interpret as there is also some interplay between the minor cations in their elemental distribution. The elemental distribution is probably influenced by a complex range of factors such as pH, temperature, pCO_2 and saturation. The morphological compositional heterogeneity within sphaerosiderites suggests they may have been growing close enough to the soil surface to record physiochemical changes of pore waters. Although in a few cases extensive substitution of minor cations is notable, in most cases, siderite was verifiable by XRD, and lack of diagenetic alteration textures with Mg substitution suggest the siderites were not produced from recrystallisation and/or post-burial overgrowths. The presence of calcite in two horizons, dissolution textures within a few horizons, and regional recrystallisation of the Wadhurst Clay sphaerosiderites have been tentatively interpreted as indicating periods of marine or brackish influence within the basin. The heterogeneous elemental and morphological compositions within individual spheres suggests spatially and temporally varying physiochemical conditions during growth of individual spheres, and aligns with the sedimentological evidence from the Weald Basin suggesting the wetland system was a variable and dynamic environment with humid conditions, frequent storms and groundwater recharging.




ACKNOWLEDGEMENTS

This study was funded by NERC as part of the Doctoral Training Partnership in Environmental Research at the University of Oxford (NE/L002612/1). The authors would like to thank Alice Barroll, Kat Clayton, Jon Wade, Phil Gopon, John Craven, Jon Wells, and Rebecca Smith for assistance with analyses and sample preparation.

DATA AVAILABILITY STATEMENT

The main data that support the findings of this study are available as supplementary information and supplementary data. Any further data requests can be made to the corresponding author and will be made available upon reasonable request.

ORCID

Ritwika Sengupta  <https://orcid.org/0000-0001-5349-994X>
 Stuart A. Robinson  <https://orcid.org/0000-0003-4329-1058>
 Nicholas J. Tosca  <https://orcid.org/0000-0003-4415-4231>

REFERENCES

- Allen, P. (1975) Wealden of the Weald: a new model. *Proceedings of the Geologists' Association*, 86, 389–437.
- Allen, P. (1981) Pursuit of Wealden models. *Journal of the Geological Society of London*, 138, 375–405.
- Allen, P. (1989) Wealden research—ways ahead. *Proceedings of the Geologists' Association*, 100, 529–564.
- Allen, P., Alvin, K.L., Andrews, J.E. & Batten, D.J. (1998) Purbeck-Wealden (early Cretaceous) climates. *Proceedings of the Geologists' Association*, 109, 197–236.
- Allen, P. & Wimbledon, W.A. (1991) Correlation of NW European Purbeck-Wealden (nonmarine Lower Cretaceous) as seen from the English type-areas. *Cretaceous Research*, 12(5), 511–526.
- Batten, D.J. (1982) Palynofacies and salinity in the Purbeck and Wealden of southern England. In: Banner, F.T. & Lord, A.R. (Eds.) *Aspects of micropalaeontology*. Dordrecht: Springer, pp. 278–308. https://doi.org/10.1007/978-94-011-6841-0_8
- Batten, D.J. (1998) Palaeoenvironmental implications of plant, insect and other organic-walled microfossils in the Weald Clay Formation (Lower Cretaceous) of southeast England. *Cretaceous Research*, 19, 279–315.
- Batten, D.J. & Lister, J.K. (1988) Evidence of freshwater dinoflagellates and other algae in the English Wealden (Early Cretaceous). *Cretaceous Research*, 9, 171–179.
- Berner, R.A. (1971) *Principles of chemical sedimentology*. New York: McGraw Hill.
- Berner, R.A. (1983) Sedimentary pyrite formation. *Geochimica Cosmochimica Acta*, 48, 605–615.
- Bojanowski, M.J., Goryl, M., Kremer, B., Marciniak-Maliszewska, B., Marynowski, L. & Śródoń, J. (2020) Pedogenic siderites fossilizing Ediacaran soil microorganisms on the Baltica paleocontinent. *Geology*, 48(1), 62–66.
- Busenberg, E., Plummer, L.N. & Mumpston, F.A. (1986) A comparative study of the dissolution and crystal growth kinetics of calcite and aragonite. *Studies in Diagenesis: USGS Bulletin*, 1578, 139–168.
- Carothers, W.W., Adami, L.H. & Rosenbauer, R.J. (1988) Experimental oxygen isotope fractionation between side&-water and phosphoric acid liberated CO₂-siderite. *Geochimica et Cosmochimica Acta*, 52, 2445–2450.
- Choi, K.S., Khim, B.K. & Woo, K.S. (2003) Spherulitic siderites in the Holocene coastal deposits of Korea (eastern Yellow Sea): elemental and isotopic composition and depositional environment. *Marine Geology*, 202, 17–31.
- Choi, K. & Kim, S.P. (2006) Late Quaternary evolution of macrotidal Kimpo tidal flat, Kyonggi Bay, west coast of Korea. *Marine Geology*, 232, 17–34.
- Coleman, M.L. (1993) Microbial processes: controls on the shape and composition of carbonate concretions. *Marine Geology*, 113, 127–140.
- Coleman, M.L., Hedrick, D.B., Lovley, D.R., White, D.C. & Pye, K. (1993) Reduction of Fe(III) in sediments by sulphate-reducing bacteria. *Nature*, 361, 436–438.
- Driese, S.G., Ludvigson, G.A., Roberts, J.A., Fowle, D.A., González, L.A., Smith, J.J., Vulava, V.M. & McKay, L.D. (2010) Micromorphology and stable-isotope geochemistry of historical pedogenic siderite formed in PAH-contaminated alluvial clay soils, Tennessee, USA. *Journal of Sedimentary Research*, 80, 943–954.
- Fernandez, A., Tang, J. & Rosenheim, B.E. (2014) Siderite “clumped” isotope thermometry: a new paleoclimate proxy for humid continental environments. *Geochimica et Cosmochimica Acta*, 126, 411–421.
- Fisher, Q.J., Raiswell, R. & Marshall, J.D. (1998) Siderite concretions from nonmarine shales (Westphalian A) of the Pennines, England: controls on their growth and composition. *Journal of Sedimentary Research*, 68, 1034–1045.
- Geology of Britain B. G. S. (2016) Geology of Britain BGS. Available at: <https://mapapps.bgs.ac.uk/geologyofbritain/home.html>
- Haywood, A.M., Valdes, P.J. & Markwick, P.J. (2004) Cretaceous (Wealden) climates: a modelling perspective. *Cretaceous Research*, 25, 303–311.
- Horne, D.J. (1995) A revised ostracod biostratigraphy for the Purbeck-Wealden of England. *Cretaceous Research*, 16, 639–663.
- Jiang, C.Z. & Tosca, N.J. (2020) Growth kinetics of siderite at 298.15 K and 1 bar. *Geochimica et Cosmochimica Acta*, 274, 97–117.
- Jimenez-Lopez, C. & Romanek, C.S. (2004) Precipitation kinetics and carbon isotope partitioning of inorganic siderite at 25°C and 1 atm. *Geochimica et Cosmochimica Acta*, 68, 557–571.
- Kantorowicz, J.D. (1985) The petrology and diagenesis of Middle Jurassic clastic sediments, Ravenscar Group, Yorkshire. *Sedimentology*, 32, 833–853.
- Khim, B.-K., Choi, K.-S. & Park, Y.A. (2000) Elemental composition of siderite grains in early-Holocene deposits of Youngjong Island (west coast of Korea), and its palaeoenvironmental implications. *Proceedings of the Marine Science*, 2, 205–217.
- Khim, B.-K., Choi, K.-S., Park, Y.-A. & Oh, J.-K. (1999) Occurrence of authigenic siderites in the Early Holocene coastal deposit in the west coast of Korea: an indicator of depositional environment. *Geosciences Journal*, 3, 163–170.
- Lake, R. (1969) Record of Shaft or Borehole – Cooden No. 1. http://scans.bgs.ac.uk/sobi_scans/boreholes/584545/images/12204638.html
- Lin, C.Y., Turchyn, A.V., Krylov, A. & Antler, G. (2019) The microbially driven formation of siderite in salt marsh sediments. *Geobiology*, 18, 1–18.
- Lin, C.Y., Turchyn, A.V., Steiner, Z., Bots, P., Lampronti, G.I. & Tosca, N.J. (2018) The role of microbial sulfate reduction in calcium carbonate polymorph selection. *Geochimica et Cosmochimica Acta*, 237, 184–204.
- Ludvigson, G.A., González, L.A., Fowle, D.A., Roberts, J.A., Driese, S.G., Villarreal, M.A., Smith, J.J. & Suarez, M.B. (2013) Paleoclimatic applications and modern process studies of pedogenic siderite. In: Driese, S.G. & Nordt, L.C. (Eds.) *New frontiers in paleopedology and terrestrial paleoclimatology*, SEPM Special Publication. SEPM (Society for Sedimentary Geology), 104, pp. 79–87. <https://doi.org/10.2110/sepm104>
- Ludvigson, G.A., González, L.A., Metzger, R.A., Witzke, B.J., Brenner, R.L., Murillo, A.P. & White, T.S. (1998) Meteoric sphaerosiderite lines and their use for paleohydrology and paleoclimatology. *Geology*, 26, 1039–1042.
- Mitsch, W. & Gosselink, J. (2015) *Wetlands*, 5th edition. Hoboken, New Jersey: John Wiley and Sons.
- Mitsch, W.J., Nahlik, A., Wolski, P., Bernal, B., Zhang, L. & Ramberg, L. (2010) Tropical wetlands: seasonal hydrologic pulsing, carbon sequestration, and methane emissions. *Wetlands Ecology and Management*, 18, 573–586.

- Moore, S.E., Ferrell, R.E. & Aharon, P. (1992) Diagenetic siderite and other Ferroan carbonates in a modern subsiding marsh sequence. *SEPM Journal of Sedimentary Research*, 62, 357–366.
- Morter, A.A. (1984) Purbeck-Wealden Beds Mollusca and their relationship to ostracod biostratigraphy, stratigraphical correlation and palaeoecology in the Weald and adjacent areas. *Proceedings of the Geologists' Association*, 95(3), 217–234.
- Mortimer, R.J.G., Coleman, M.L. & Rae, J.E. (1997) Effect of bacteria on the elemental composition of early diagenetic siderite: implications for palaeoenvironmental interpretations. *Sedimentology*, 44, 759–765.
- Mozley, P.S. (1989) Relation between depositional environment and the elemental composition of early diagenetic siderite. *Geology*, 17, 704–706.
- Mozley, P.S. & Carothers, W.W. (1992) Elemental and isotopic composition of siderite in the Kuparuk Formation, Alaska: effect of microbial activity and water/sediment interaction on early pore-water chemistry. *SEPM Journal of Sedimentary Research*, 62, 681–692.
- Mozley, P.S. & Wersin, P. (1992) Isotopic composition of siderite as an indicator of depositional environment. *Geology*, 20, 817–820.
- Passey, S.R. (2014) The habit and origin of siderite spherules in the Eocene coal-bearing Prestfjall Formation, Faroe Islands. *International Journal of Coal Geology*, 122, 76–90.
- Postma, D. (1980) Formation of siderite and vivianite and the pore-water composition of a recent bog sediment in Denmark. *Chemical Geology*, 31, 225–244.
- Pye, K. (1984) SEM analysis of siderite cements in intertidal marsh sediments, Norfolk, England. *Marine Geology*, 56, 1–12.
- Pye, K., Dickson, J.A.D., Schiavon, N., Coleman, M.L. & Cox, M. (1990) Formation of siderite-Mg-calcite-iron sulphide concretions in intertidal marsh and sandflat sediments, north Norfolk, England. *Sedimentology*, 37, 325–343.
- Radley, J.D. (1994) Stratigraphy, palaeontology and palaeoenvironment of the Wessex Formation (Wealden Group, Lower Cretaceous) at Yaverland, Isle of Wight, southern England. *Proceedings of the Geologists' Association*, 105, 199–208.
- Radley, J.D. (2006a) A Wealden guide I: the Weald Sub-basin. *Geology Today*, 22, 109–118.
- Radley, J.D. (2006b) A Wealden guide II: the Wessex Sub-basin. *Geology Today*, 22, 187–193.
- Radley, J.D. & Allen, P. (2012) The non-marine Lower Cretaceous Wealden strata of southern England. *Proceedings of the Geologists' Association*, 123, 235–244.
- Robinson, S.A., Andrews, J.E., Hesselbo, S.P., Radley, J.D., Dennis, P.F., Harding, I.C. & Allen, P. (2002) Atmospheric pCO₂ and depositional environment from stable-isotope geochemistry of calcrite nodules (Barremian, Lower Cretaceous, Wealden Beds, England). *Journal of the Geological Society of London*, 159, 215–224.
- Robinson, S.A., Scotchman, J.I., White, T.S. & Atkinson, T.C. (2010) Constraints on palaeoenvironments in the Lower Cretaceous Wealden of southern England, from the geochemistry of sphaerosiderites. *Journal of the Geological Society of London*, 167, 303–311.
- Rollion-Bard, C. & Marin-Carbonne, J. (2011) Determination of SIMS matrix effects on oxygen isotopic compositions in carbonates. *Journal of Analytical Atomic Spectrometry*, 26, 1285–1289.
- Romanek, C.S., Jiménez-López, C., Navarro, A.R., Sánchez-Román, M., Sahai, N. & Coleman, M. (2009) Inorganic synthesis of Fe-Ca-Mg carbonates at low temperature. *Geochimica et Cosmochimica Acta*, 73, 5361–5376.
- Sengupta, R., Tosca, N.J. & Robinson, S.A. (2020) Geochemical controls on the elemental composition of siderite: implications for palaeo-environmental reconstructions. *Geochimica et Cosmochimica Acta*, 271, 1–15.
- Shephard-Thorn, E., Lake, R. & Hildreth, P. (1971) Record of shaft or borehole – fairlight. http://scans.bgs.ac.uk/sobi_scans/boreholes/614078/images/12547057.html
- Steinmann, P. & Shotyk, W. (1997) Chemical composition, pH, and redox state of sulfur and iron in complete vertical porewater profiles from two Sphagnum peat bogs, Jura Mountains, Switzerland. *Geochimica et Cosmochimica Acta*, 61, 1143–1163.
- Suarez, M.B., González, L.A. & Ludvigson, G.A. (2010) Estimating the oxygen isotopic composition of equatorial precipitation during the mid-Cretaceous. *Journal of Sedimentary Research*, 80, 480–491.
- Thorley, S. (1969) Record of shaft or borehole – Westfield. British Geological Survey. <https://www.bgs.ac.uk/data/boreholescans/home.html>
- Thornber, M.R. & Nickel, E.H. (1976) Supergene alteration of sulphides. III. The composition of associated carbonates. *Chemical Geology*, 17, 45–72.
- Ufnar, D.F., González, L.A., Ludvigson, G.A., Brenner, R.L. & Witzke, B.J. (2004a) Evidence for increased latent heat transport during the Cretaceous (Albian) greenhouse warming. *Geology*, 32(12), 1049–1052.
- Ufnar, D.F., Gonzalez, L.A., Ludvigson, G.A., Brenner, R.L. & Witzkes, B.J. (2004b) Diagenetic overprinting of the sphaero-siderite palaeoclimate proxy: are records of pedogenic groundwater $\delta^{18}\text{O}$ values preserved? *Sedimentology*, 51, 127–144.
- Van Dijk, J., Fernandez, A., Storck, J.C., White, T.S., Lever, M. & Müller, I.A. (2019) Experimental calibration of clumped isotopes in siderite between 8.5 and 62°C and its application as paleo-thermometer in paleosols. *Geochimica et Cosmochimica Acta*, 254, 1–20.
- Watson, J. & Alvin, K.L. (1996) An English Wealden floral list, with comments on possible environmental indicators. *Cretaceous Research*, 17, 5–26.
- Weibel, R., Lindstrom, S., Pedersen, G.K., Johansson, L., Dybkjor, K., Whitehouse, M.J., Boyce, A.J. & Leng, M.J. (2016) Groundwater table fluctuations recorded in zonation of microbial siderites from end-Triassic strata. *Sedimentary Geology*, 342, 45–65.
- Worssam, B.C. & Morter, A.A. (1978) The stratigraphy of the Weald Clay., Institute of Geological Sciences. *Report 78/11*, 1–23.
- Wright, V.P., Taylor, K.G. & Beck, V.H. (2000) The Paleohydrology of Lower Cretaceous seasonal wetlands, Isle of Wight, Southern England. *Journal of Sedimentary Research*, 70, 619–632.

SUPPORTING INFORMATION

Additional supporting information may be found online in the Supporting Information section.

How to cite this article: Sengupta R, Robinson SA, Tosca NJ. Sphaerosiderites as sensitive recorders of non-marine depositional and diagenetic history: Insights from the Lower Cretaceous Wealden Supergroup. *Depositional Rec.* 2021;7:520–540. <https://doi.org/10.1002/dep2.164>